Physik Department

MOLECULAR & CELLULAR BIOPHYSICS

Abschlussarbeit im Masterstudiengang Physik

# Photophysical Characterization of GFP Variants by Single-Molecule Spectroscopy and Microscopy

**Photophysikalische Charakterisierung von GFP-Varianten mit Einzelmolekülspektroskopie und -mikroskopie**

Frederik Steiert

1st December 2016

Technische Universität München

Primary supervisor: Prof. Dr. Matthias Rief
Secondary supervisor: Prof. Dr. Petra Schwille

# Contents


**1. Introduction** **1**

1.1. General Context . . . . . 1
1.2. The Biochemistry of Green Fluorescent Proteins . . . . . 2
1.3. The Structure of Green Fluorescent Proteins . . . . . 3
1.4. Photodynamics of Green Fluorescent Proteins . . . . . 6
1.5. Aim of this Study . . . . . 7

**2. Material and Methods** **8**

2.1. Fluorescence and Photophysics . . . . . 8
2.2. Fluorescence Correlation Spectroscopy (FCS) . . . . . 8
2.2.1. Setup . . . . . 10
2.2.2. Data Acquisition . . . . . 11
2.2.3. Data Analysis . . . . . 11
2.3. Total Internal Reflection Fluorescence (TIRF) Microscopy . . . . . 14
2.3.1. Single-Molecule Imaging . . . . . 15
2.3.2. Data Analysis . . . . . 16
2.4. Fluorescence Lifetime Measurements . . . . . 16
2.5. Preparation and Purification of mNeonGreen Oligomers . . . . . 17

**3. Steady-State Fluorescence Spectra of GFP constructs** **21**

**4. TIRF Microscopy of Immobilized GFPs** **22**

4.1. Photostability of mNeonGreen, EGFP and AcGFP . . . . . 22
4.2. Non-Fluorescent Fractions of mNeonGreen . . . . . 25

**5. Fluorescence Spectroscopy of Monomeric GFP Variants** **30**

5.1. Molecular Brightness of mNeonGreen, EGFP and AcGFP . . . . . 30
5.1.1. Power Series in a Diffraction-Limited Focus Volume . . . . . 30
5.1.2. Power Series with an Enlarged Focus Volume . . . . . 33
5.2. Fluorescence Lifetime Measurements . . . . . 34
5.3. Triplet and Blinking Dynamics of the GFP Variants . . . . . 37
5.4. Protonation of the Chromophore . . . . . 37

**6. Fluorescence Spectroscopy of mNeonGreen Tandem Proteins** **43**
6.1. Diffusional Properties of mNeonGreen Oligomers . . . . . 43
6.2. Effect of Oligomerization on Molecular Brightness . . . . . 47
6.3. Effect of Oligomerization on Fluorescence Lifetime . . . . . 49
6.4. Blinking Dynamics in Multimerized mNeonGreen . . . . . 50

**7. Conclusion** **53**

**A. Appendix** **55**
A.1. TIRFM . . . . . 55
A.2. FCS . . . . . 56

**Bibliography** **57**

**Acknowledgements** **60**

# List of Figures


1.1. Crystal structures of EGFP, AcGFP and laGFP . . . . . 3
1.2. Overlay of the crystal structures of GFPs . . . . . 4

2.1. Jablonski diagram . . . . . 8
2.2. Confocal microscope-based FCS setup . . . . . 11
2.3. Simulation of a T-T-3D model correlation function . . . . . 12
2.4. Preparation and purification of mNeonGreen oligomers . . . . . 19
2.5. Sequence alignment of the characterized monomeric GFP variants. . . . 20

3.1. Absorption and emission spectra of mNeonGreen, EGFP and AcGFP . . 21

4.1. Single-molecule TIRF images . . . . . 23
4.2. Photostability of the GFPs in bulk . . . . . 24
4.3. Photostability of monomeric and trimeric mNeonGreen . . . . . 25
4.4. Time courses of fluorescence emission showing step-wise bleaching . . . 26
4.5. Distribution of number of steps observed in mNeonGreen single-molecule photobleaching analysis. . . . . 27
4.6. Distribution of step-wise intensity drops for monomeric and trimeric mNeonGreen . . . . . 28

5.1. Effect of the excitation intensity and focus volume size on ACFs of mNeonGreen, EGFP and AcGFP. . . . . 31
5.2. Molecular brightness of freely diffusing GFP monomers . . . . . 32
5.3. Molecular brightness of freely diffusing GFPs as measured in FCS at different laser powers with an enlarged focus volume. . . . . 35
5.4. Fluorescence lifetime of GFP monomers measured with TCSPC-FLIM. . 36
5.5. Power dependence of blinking fraction and blinking time for mNeonGreen, EGFP and AcGFP. . . . . 37
5.6. Exemplary correlation curves showing the effect of different pH on mNeonGreen, EGFP and AcGFP. . . . . 40
5.7. mNeonGreen's sensitivity to varying pH differs strongly from EGFP and AcGFP regarding blinking fraction and molecular brightness. . . . . 41
5.8. Blinking is not related to a diffusional process. . . . . 41

5.9. Interdependency of blinking fraction and blinking time on laser irradiance and pH. . . . . 42

6.1. Exemplary correlation curves of monomeric and pentameric mNeonGreen. 44
6.2. Diffusion coefficient of mNeonGreen oligomers in the low irradiance regime observed in FCS. . . . . 45
6.3. Diffusional properties of mNeonGreen oligomers in the nucleus and cytoplasm. . . . . 46
6.4. Molecular brightness of mNeonGreen oligomers . . . . . 48
6.5. Molecular brightness of mNeonGreen oligomers in the nucleus and cytoplasm. . . . . 49
6.6. Fluorescence lifetime of mNeonGreen chain *in vitro* and *in vivo* . . . . . 51
6.7. Homo-FRET increases slightly with chain length in mNeonGreen tandems . . . . . 52
6.8. Dependence of blinking amplitude and blinking time on excitation intensity for mNeonGreen oligomers . . . . . 52

A.1. TIRF images of mNeonGreen oligomers. . . . . 55
A.2. Triplet fraction and time of monomeric GFPs and the mNeonGreen chain. 56

# 1. Introduction

## 1.1. General Context

Fluorescence microscopy plays an important role in life sciences. The ability to selectively observe fluorescently tagged proteins above a background of thousands of endogenous proteins expanded our knowledge about the spatiotemporal regulation of proteins in living cells. A key enabling technology represents the possibility to genetically fuse a fluorescent protein (FP) domain as a marker to any protein of interest. FP-labeling can be done from 'inside' the cell, without the need to penetrate the cell boundary with chemicals or enzymes. Straightforward DNA recombination technology allowed the comparably easy manipulation of cloned genes of interest within a vector plasmid and their expression in target cells or tissues. Subsequently, genetic FP-labeling catalyzed a wide spectrum of fluorescence based microscopic technologies to study proteins in living cells.

It is a serious inherent limitation of conventional fluorescence imaging under wide field and confocal illumination that the strength of the signals depends on the applied excitation, i.e. the intensity of lamp or laser light used to excite the fluorescent sample. Thus, images cannot be interpreted in molecular terms without laborious calibrations (Weidemann, Wachsmuth et al., 2003). Although confocal microscopy in combination with fluorescence fluctuation analysis provides a means to interpret signal fluctuations in terms of molecular parameters, these advanced techniques are limited to freely diffusing fluorescent molecules in the volume where the laser focus is positioned (Weidemann, Mücksch and Schwille, 2014). Such quasi-equilibrium conditions are rarely given in cells that feature a considerable degree of spatial heterogeneity. Many biochemical processes are either transient and precisely regulated in time or they occur in specialized compartments like small vesicles or supramolecular aggregates. In addition, imaging is limited by sensitivity in general. Cellular processes that involve only a couple of molecules per diffraction limited voxel are basically invisible when employing FP-labeling. Since the advent of green fluorescent protein (GFP) in the early nineties of the last century, the field therefore invested continuous efforts for improving the photophysical properties of fluorescent protein variants.

## 1.2. The Biochemistry of Green Fluorescent Proteins

The wilde-type GFP (wtGFP) isolated from *Aequorea victoria* has been studied for about two decades before the crystal structures were finally reported (Ormo et al., 1996; Yang, Moss and Phillips, 1996). Purified GFP is a very stable protein that can resist harsh denaturing conditions like 6 M guanidinium hydrochloride (chemical similar to the arginine side chain) at 90 °C. It remains fluorescent under a broad range of different pH (4<pH<12). Partial unfolding seems to be reversible, as the fluorescent signal recovers within minutes following reversal of denaturing conditions by dialysis or neutralization (Ward and Bokman, 1982). Maturation time for wtGFP is about 4 hours. Temperatures higher than 30 °C seem to be unfavorable for maturation, therefore some laboratories cultivated cells for protein production at temperatures lower than 37 °C (Yang, Moss and Phillips, 1996). Nonspecific proteolysis (papain) leads to a residual chromopeptide containing the chromophore (Cody et al., 1993). Similar to intact wtGFP protein, these chromopeptides absorb at shorter wavelength (360 nm) in buffer of pH 4 and at longer wavelengths (450 nm) in buffer of pH 11 with an isosbestic point at 405 nm. However, these chromopeptides are themselves non-fluorescent, indicating that shielding of the chromophore by the protein shell is crucial for light emitting properties.

In wtGFP, absorption spectra show two peaks that are associated with two electronic systems corresponding to two isoforms of the chromophore. The two electronic systems can be interconverted by irradiance with UV-light. Within minutes, the 395 nm absorption peak decreases with a concomitant increase of the 475 nm absorption peak (Chattoraj et al., 1996; Cubitt et al., 1995). This photo-isomerization reaction seems irreversible when using 280 nm irradiation (Cubitt et al., 1995), whereas 60% recovery was observed after 24 hours in the dark when using 398 nm for photo-conversion (Chattoraj et al., 1996). In the GFP-S65T mutant (amino acids in one letter code) the 395 nm absorption band is missing at higher pH. Although here absorption at 395 nm builds up under acidic conditions, the band is always non-fluorescent for detection at 500 nm. In GFP-S65T, the absorption cross-section of the longer wavelength band (with a maximum at 475 nm in wtGFP) is significantly increased and the maximum for the S65T mutant shifted to 488 nm (Cubitt et al., 1995). This drastic effect occurs although the hydroxyl group is shifted only one carbon further (from gamma-position in T65 to beta-position in S65). Accordingly, the GFP-S65T substitution in combination with F64L that improves folding was termed enhanced GFP (EGFP) and soon recognized as a superior candidate for genetic fluorescence labeling applications (Cubitt et al., 1995).

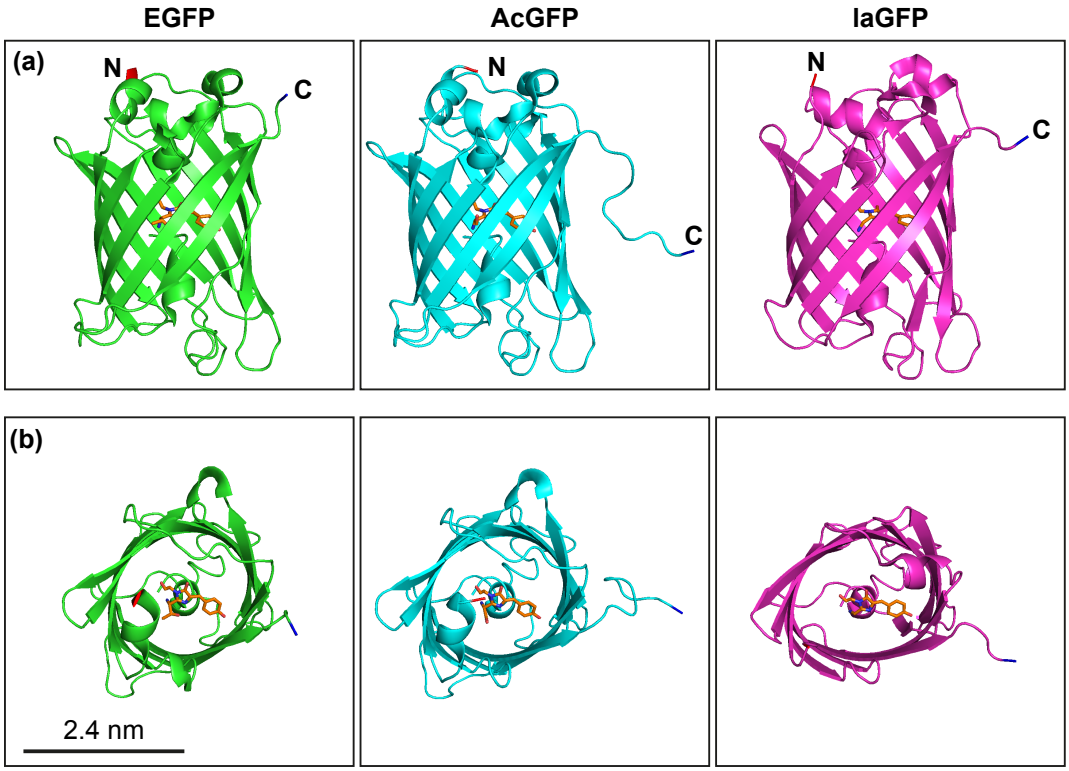


**Figure 1.1.:** Crystal structures of EGFP (PDB: 2Y0G), AcGFP (PDB: 3LVA), and laGFP (PDB: 4HVF), a precursor protein of mNeonGreen, visualized from similar angles in (a) side view and (b) from the top, where the N- and C-termini are indicated. The secondary structures were illustrated using the style "cartoon", the chromophore is shown in orange "stick" representation (MacPyMOL: PyMOL v1.8.0.3, enhanced for MacOS). In comparison to EGFP and AcGFP, the barrel of laGFP appears flattened.

## 1.3. The Structure of Green Fluorescent Proteins

The crystal structure of GFP revealed immediately the compact architecture of the protein shell around the chromophore. The GFP structure consist of an 11 stranded beta-barrel (beta-can) 3 nm wide and 4 nm high (Yang, Moss and Phillips, 1996) or rather 2.4 nm wide and 4.2 nm high as Ormö et al. reported for GFP-S65T (Ormo et al., 1996). The N- and C-terminus exit at the same face of the barrel (fig. 1.1). Both faces of the barrel appear capped with small alpha-helical domains. Three amino acids (S65, T66, and G67 for wtGFP) covalently form the chromophore, a hydroxbenzylidene-imidazolinone moiety providing the conjugated $\pi$-electron system for fluorescence, positioned within a central alpha-helix at a 60° angle with respect to the length axis of the barrel (fig. 1.2a).

The required cyclization reaction is a result of protein folding, therefore autocatalytic in nature and requires dioxygen in a final maturation step. Mass spectrometry indicated in 30% of GFP-S65T protein a surplus of 18-20 Da. This mass difference

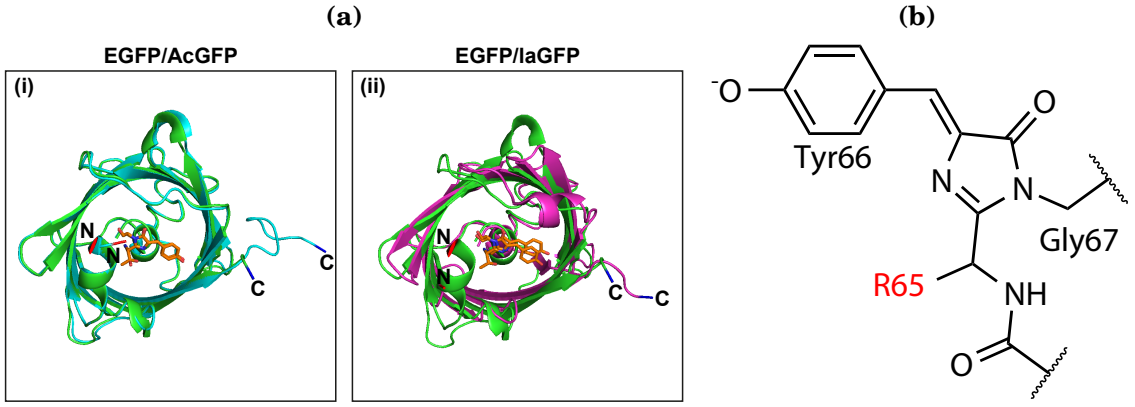


**Figure 1.2.:** Overlay of crystal structures (i) EGFP (green, PDB: 2Y0G) and AcGFP (turquoise, PDB: 3LVA) and (ii) EGFP and laGFP (violet, PDB: 4HVF) visualized from the top, where the N-termini (red) and C-termini (blue) are indicated. The position of the chromophore of EGFP and AcGFP is almost identical reflecting the high degree of homology (21 amino acid substitutions), but shifted with respect to mNeonGreen.
(b) Chemical structure of the main type of chromophores in green fluorescent proteins highlighting the amino acid side-chain in red at position 65, which differs among the three GFP variants under investigation.

corresponds to exactly one water molecule (Ormo et al., 1996). Since water is supposed to be lost during cyclization, this finding suggested that only 70% of the purified GFP-S65T variant have matured into a fluorescent form. Ormö et al. describe a large cavity where four water molecule are buried linking E222 and Q69 by a chain of H-bonds in the vicinity of the chromophore (Ormo et al., 1996). It is speculated that one of these water molecules is produced by the dehydration reactions during cyclization and that the cavity accommodates dioxygen used for the final maturation step. Yang et al. emphasize the paradoxical role of dioxygen: on one hand it is required for maturation, a dehydration reaction that generates the double bond between the $C_\alpha$ and $C_\beta$ of Y66, on the other hand oxygen is a dangerous quenching reagent for the matured chromophore. GFP-evolution may therefore have sacrificed 100% maturation efficiency for improved stability and quantum yield once it is fully formed (Yang, Moss and Phillips, 1996).

Quite interesting, GFP cannot be much further reduced to a minimal fluorescent protein. Genetic deletions further than the N-terminal methionine (position 1) as well as chopping more than 7 amino acids from the C-terminus (positions 231-238) abolishes fluorescence (Dopf and Horiagon, 1996). In the structure of wtGFP, the 7 C-terminal amino acids appear unstructured. Their lacking role in stabilizing the barrel structure may explain why these amino acids appear superfluous for fluorescence, however, the crucial role of the N-terminus for fluorescence is less clear. N-terminal amino acids seem to contribute in capping the beta-barrel for tight chemical shield-

| | mNeonGreen | EGFP | AcGFP |
|---|---|---|---|
| Excitation wavelength [nm] | 506 | 488 | 475 |
| Emission wavelength [nm] | 517 | 507 | 505 |
| Extinction coefficient [$M^{-1}$ $cm^{-1}$] | 116 000 | 56 000 | 32 500 |
| Quantum yield (QY) | 0.8 | 0.6 | n.d. |
| Brightness (EC·QY) | 92.8 | 33.6 | n.d. |
| Fluorescence lifetime [ns] | n.d. | ≈ 2.5 | n.d. |
| Chromophore sequence | GYG | TYG | SYG |

**Table 1.1.: Published fluorescence properties of GFP variants.**

ing. Crystal structures indeed provide hints that the stability of the chromophore environment is crucial for fluorescence. Yang at al. stress the unusual accumulation of charged amino acids in the vicinity of the chromophore, which show extensive hydrogen-bonding to electronegative atoms of the chromophore (Yang, Moss and Phillips, 1996). The comparably small Stokes-shift of GFPs was explained by the rigid encapsulation of the chromophore that prevents dissipative vibrations during the excited state (Ormo et al., 1996). In both wtGFP and the S65T mutant, there is a single tryptophan buried in the neighborhood of the chromophore that shows no emission by its own, potentially due to resonance energy transfer (RET). It was suggested that polarization of aromatic residues in the vicinity of the chromophore can dissipate excited state energy and lead to red shifted variants, as exemplified by the T203Y mutation leading to enhanced yellow fluorescent protein (EYFP).

Our three protein candidates under investigation contain three different combinations of amino acids involved in the cyclization reaction: in AcGFP (as in wtGFP) 'SYT', in EGFP 'TYG' and in mNeonGreen (as in EYFP) 'GYG' (table 1.1). Due to the different chromophore chemistry diverse photophysical properties can be expected. However, to causally link protein sequence to photophysics is not as straightforward as it seems. Because polarization of the chromophore is an important feature to interpret spectroscopic data, hydrogen bonding and the location of negative charges was extensively discussed for the crystal structure of GFP-S65T. Side chains of amino acids surrounding the chromophore keep three essential oxygen atoms negatively charged: (i) the phenolic hydroxyl of Y66 by T203, H148, and S205, (ii) the side chain oxygen of T65 (in the S65T mutant) by E222, and (iii) the carbonyl oxygen of the imidazolidinone ring by R96. Contrary to the S65T mutation that abolishes the 395 nm absorption band, a hydrophobic isoleucine replacement T203I abolishes the 488 nm peak in the excitation spectrum. Thus, 488 nm excitation seems to require a negative charge locating at Y66.

## 1.4. Photodynamics of Green Fluorescent Proteins

In agreement with photo-conversion experiments, time-resolved spectroscopy already showed quite rich photophysical phenomena and the existence of multiple substates and isoforms were suggested for wtGFP (Chattoraj et al., 1996). Interestingly, these experiments promoted a mechanism by which the two isoforms interconvert preferentially via the excited state, a process that involves protonation of the chromophore. Because the isoform of the 395 nm absorption band is non-fluorescent in GFP-S65T, a modified dark-state-model was employed to explain fast flickering of the fluorescence signal in fluorescence correlation spectroscopy (FCS) experiments (Haupts et al., 1998). Measuring purified GFP in buffers of varying pH, this seminal study proposed that external protonation of the terminal hydroxyl group in Y66 drives the GFP molecules into a transient dark state (lasting 50-500 µs). Since the fraction of molecules in the dark state decreased to a constant plateau at basic conditions, a competing 'internal' protonation reaction was also proposed. Importantly, substituting Y66 with a non-polar tryptophan abolished the entire blinking phenomenon and thus provided a strong argument for role of protonation for these transitions. A follow-up FCS study along similar lines investigated YFP variants and uncovered additional, photo-induced isomerization reactions. On the timescale of microseconds a fluorescent and dark state interconvert exclusively via their excited states as a gateway (Schwille et al., 2000). Thus, depending on chromophore structure, protonation and photo-induced isomerization might be coupled, therefore adding considerable complications for the interpretation of molecular brightness in different chemical environments.

The blinking behavior of EGFP was thouroughly studied by Widengren and Rigler, who provided pioneering work on the treatment of triplet transitions (Widengren, Mets and Rigler, 1999). Measuring pseudo-cross-correlation over an extended time range from 12.5 ns to 1 s allowed even to resolve signal contributions associated with rotational movement (19 ns). Widengren determined the fundamental anisotropy of GFP(S65T) to be $r_0 = 0.39$, thus confirming the rigid embedding of the chromophore within the GFP-barrel. Concerning blinking, the authors claim a complex blinking behavior that involves three time scales: (i) very fast blinking (2 µs, 10%) that is only visible at very high laser powers, however, excitation independent and therefore not associated with triplet, (ii) intermediate blinking ($500 - 10$ µs; 14%) that is associated with photo-induced isomerization (ISO1), and (iii) a blinking time in the range of $100\,\mu s - 5$ ms that is associated with another photo-induced isomerization state (ISO2). Surprisingly, diffusion times fall in the same range as transition into ISO2 and it is not clear how they can be distinguished in the fit. Varying the pH

in a range between 6 and 4.5 revealed fundamental differences between FITC and EGFP (Widengren, Terry and Rigler, 1999) For EGFP the relaxation rate depended non-linearly on the pH and buffer concentration. Also the type of buffer mattered for the magnitude of the blinking amplitude. Titration of phosphate buffers from 10 mM up to 1 M increased the relaxation rates by a factor of 10 and the steady state dark fraction of GFPs from 0.7 to 0.85 with a plateau reached already at 200 mM.

## 1.5. Aim of this Study

In the meantime, hundreds of FP mutants have been produced and described in such a rich detail that cannot be reviewed here. The search for red-shifted mutants was in particular intense due to the need for dual-color experiments that address molecular interactions between two binding partners inside cells. Available FP variants now cover the whole visible spectrum (Nathan C. Shaner, Campbell et al., 2004). Many spectral GFP variants suffered from reduced quantum yield and photostability and the search to improve these limiting properties is still ongoing (Nathan C. Shaner, Lin et al., 2008). Considering all these activities, it may appear surprising that EGFP, one of the first mutants derived from *Aequoroea victoria*, wtGFP, is still in widespread use for the familiar 488 nm argon laser line. Attempts to improve the molecular brightness have therefore been limited to multimerization of several GFP-domains (Dross et al., 2009; Pack et al., 2006; Vamosi et al., 2016). Just recently, a promising new GFP was discovered in *Brachiostoma lanceolata*, called mNeonGreen, showing an unusually high quantum yield comparable to state-of-the-art organic dyes (N. C. Shaner et al., 2013). This new GFP variant, although spectrally slightly red shifted, was proposed to be a promising candidate to replace EGFP for routine genetic labeling and live cell imaging applications.

The aim of this work is to characterize key fluorescence parameters of mNeonGreen like molecular brightness, photostability and pH sensitivity. Additionally, multimerized mNeonGreen tandem proteins were investigated. This is accomplished by the single-molecule techniques fluorescence correlation spectroscopy (FCS) in free solution and by imaging of immobilized proteins using total internal refection illumination fluorescence microscopy (TIRFM). Such data may provide a firm basis to establish mNeonGreen as a superior fluorescent marker in biophysical applications.

# 2. Material and Methods

## 2.1. Fluorescence and Photophysics

Fluorescence or photoluminescence, is the phenomenon of emitting a photon caused by the absorption of a single or multiple photons (Valeur, 2001). The process of fluorescence can be divided into three events by means of the different timescales at which they occur, as illustrated in figure 2.1. First, a molecule is excited within femtoseconds by absorption of a photon of suitable energy. As a consequence, the electron is transferred from the ground state $S_0$ to the first excited state $S_1$ or higher electronic states (singlet-singlet transition). Within picoseconds, the excess energy of higher vibrational levels is quickly relaxated. The electronic system exits the excited $S_1$ state either by emitting a fluorescence photon, or non-radiatively by internal conversion or, intersystem crossing into the triplet state.

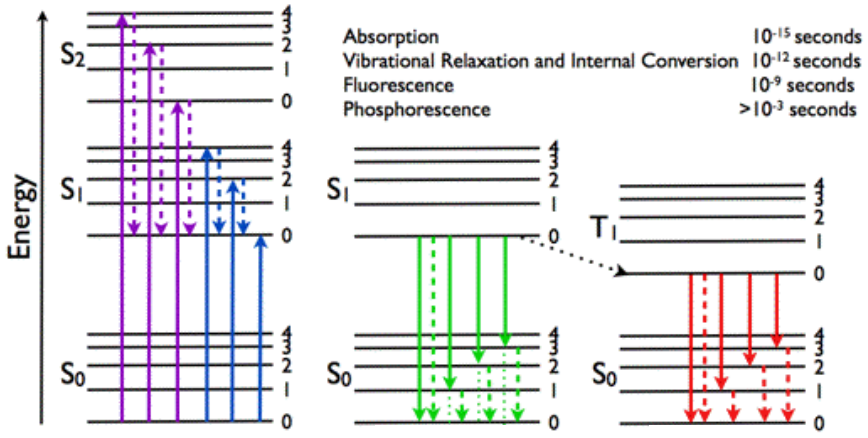


**Figure 2.1.: Jablonski diagram.**
Electronic (first subsript) and vibrational energy levels (second subsript) and the most important excitation and de-excitation pathways are shown. Dashed arrows indicate non-radiative transitions. Adapted from (Visser and Rolinski, 2014)

## 2.2. Fluorescence Correlation Spectroscopy (FCS)

In FCS, the time-dependent fluorescence signal is monitored within a small, open sample volume in solution. If the photophysical processes leading to fluorescence

are in equilibrium, the signal can be expressed as small fluctuation $\delta F(t)$ around an average fluorescence intensity $\langle F \rangle$ (Petrov and Schwille, 2008):

$$F(t) = \langle F \rangle + \delta F(t) \tag{2.1}$$

By introducing the correlation function $G(\tau)$, information inherently contained in the intensity fluctuations is extracted:

$$G(\tau) = \frac{\langle \delta F(t) \delta F(t+\tau) \rangle}{\langle F \rangle^2}. \tag{2.2}$$

The measured fluorescence intensity $F$ at a particular time $t$ can be expressed as

$$F(t) = \int W(\vec{r}) \psi c(\vec{r}, t) \mathrm{d}^3 r, \tag{2.3}$$

where $W(\vec{r})$ describes the effective shape of the detection volume, $\psi$ is the molecular brightness of the fluorophore and $c(\vec{r}, t)$ its concentration. The detection volume $W$ itself is dependent on the applied excitation intensity $I(\vec{r})$ and on the normalized collection efficiency $S(\vec{r})$ for the emitted fluorescence. The molecular brightness $\psi$ of the fluorophore is composed of the peak intensity $I_0$, the excitation cross section $\sigma_{\mathrm{exc}}$, the quantum yield QY as well as the overall detection efficiency $\kappa$ for the spectrum of emitted fluorescence:

$$W(\vec{r}) = S(\vec{r})\, I(\vec{r}) / I_0, \quad \psi = I_0 \sigma_{\mathrm{exc}} \mathrm{QY} \kappa \tag{2.4}$$

Inserting equation 2.3 into equation 2.2 gives the following analytical expression for the correlation function:

$$G(\tau) = \frac{\iint W(\vec{r}) \langle \delta c(\vec{r}, t) \delta c(\vec{r}', t+\tau) \rangle W(\vec{r}') \mathrm{d}^3 r \mathrm{d}^3 r'}{\left( \langle c \rangle \int W(\vec{r}) \mathrm{d}^3 r \right)^2} \tag{2.5}$$

This equation can be seen as the master formula of FCS, as it is the starting point for the development of model functions which describe underlying physical processes causing the signal changes.

The lateral and axial profile of the detection volume is commonly approximated by a 3D Gaussian

$$W(x, y, z) = \exp\left( \frac{-2\left(x^2 + y^2\right)}{\omega_0^2} + \frac{-2z^2}{z_0^2} \right), \tag{2.6}$$

where $\omega_0$ is the waist of the detection volume and $z_0$ its elongation along the optical axis (z-axis).

In the simplest case of pure diffusion, inserting eq. 2.6 into 2.5 yields the following correlation function for three-dimensional diffusion:

$$G(\tau) = \frac{1}{N}\left(1+\frac{\tau}{\tau_\mathrm{D}}\right)^{-1}\left(1+\frac{\tau}{(z_0/\omega_0)^2\cdot\tau_\mathrm{D}}\right)^{-1/2} = G_\mathrm{D}(\tau) \tag{2.7}$$

Here, $\tau_\mathrm{D}$ represents the characteristic residence time of a fluorophore in the detection volume and is linked to its diffusion coefficient $D$ via

$$D = \frac{\omega_0^2}{4\tau_\mathrm{D}}. \tag{2.8}$$

The average number $N$ of fluorophores inside the detection volume is, in the limit of zero lag time, equal to the inverse of the amplitude of the diffusional correlation function

$$G_\mathrm{D}(0) = \frac{1}{N}. \tag{2.9}$$

This equality can be used to access concentrations of diffusing fluorophores if the dimensions of the effective detection volume $V_\mathrm{eff}$ are known:

$$V_\mathrm{eff} = \pi^{3/2} z_0 \omega_0^2. \tag{2.10}$$

However, even for freely diffusing fluorescent particles in solution the picture is complicated by the fact that fluorophores are subject to intramolecular reactions that alter their specific brightness. In case of singlet-triplet transitions, where a fraction $T_\mathrm{trip}$ of molecules temporarily stops fluorescing, the correlation function shows an additional decay with a correlation time corresponding to the lifetime of the triplet state $\tau_\mathrm{trip}$.

$$G(\tau) = G_\mathrm{D}(\tau)\cdot G_{\mathrm{T_{trp}}}(\tau) \tag{2.11}$$

$$G(\tau) = \frac{1}{n}\left(1+\frac{\tau}{\tau_D}\right)^{-1}\left(1+\frac{\tau}{\mathrm{SP}^2\cdot\tau_D}\right)^{-1/2}\left(1+\frac{T_\mathrm{trip}}{1-T_\mathrm{trip}}\mathrm{e}^{-\tau/\tau_\mathrm{trip}}\right) \tag{2.12}$$

### 2.2.1. Setup

The FCS measurements were performed with the commercial laser scanning confocal microscope LSM780 (Carl Zeiss AG) equipped with an inverted Axio Observer.Z1 microscope and a ConfoCor 3 unit.

The excitation light of an argon ion laser operated at 488 nm is focused into the sample by a water immersion objective (C-Apochromat 40x/NA 1.2 W Korr UV-VIS-

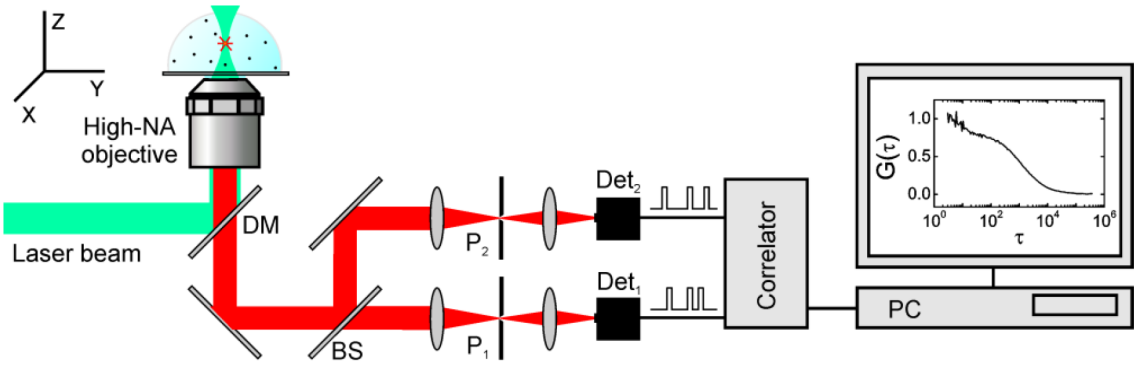


**Figure 2.2.: Sketch showing essential parts of the confocal microscope-based setup used for FCS measurements.** Adapted from Petrov and Schwille, 2008.

IR, Carl Zeiss AG). The emitted fluorescence is collected by the same objective, passes a confocal pinhole (34 µm, divided by a beam splitter (NFT IR) and subsequently detected by two avalanche photon diodes (APD). Boths beams are filtered by a long-pass (LP 505 nm) to prevent possible scattered excitation light from reaching the detectors (see fig. 2.2). The signal is correlated using multiple tau correlators, which is then displayed in realtime by the ZEN software (Carl Zeiss AG).
Even though only single-color experiments were performed throughout this study with GFPs, the separation of the fluorescence signal allows one to cross-correlate the signal from the two detectors, which removes detector artifacts like antibunching and afterpulsing from the measured correlation curves.

### 2.2.2. Data Acquisition

Each GFP construct, stored in PBS pH 7.5, was diluted to a final concentration of 15 nM in 10 mM potassium phosphate buffer with a pH value of 8 and measured in #1.5 8-well chamber cover slides (Lab-Tek, Thermo Scientific) at room temperature (≈ 23 °C). Correlation functions were recorded with an acquisition time of 30 s and repeated 30 times for each measurement. Beforehand, in a solution of ATTO488 (ATTO-TEC) the objective correction collar was adjusted to the maximum of the fluorescence signal to accommodate small thickness variation of the cover slide. In the same solution, reference measurements were calibrate the focal volume.

### 2.2.3. Data Analysis

#### Model Function

In addition to the diffusion part ($N$;$\tau_D$), the correlation curves for purified GFP variants in solution were fitted to a model containing two non-fluorescent decays: a triplet contribution ($T_{trp}$;$\tau_{trp}$) and a blinking contribution ($T_{bl}$;$\tau_{bl}$):

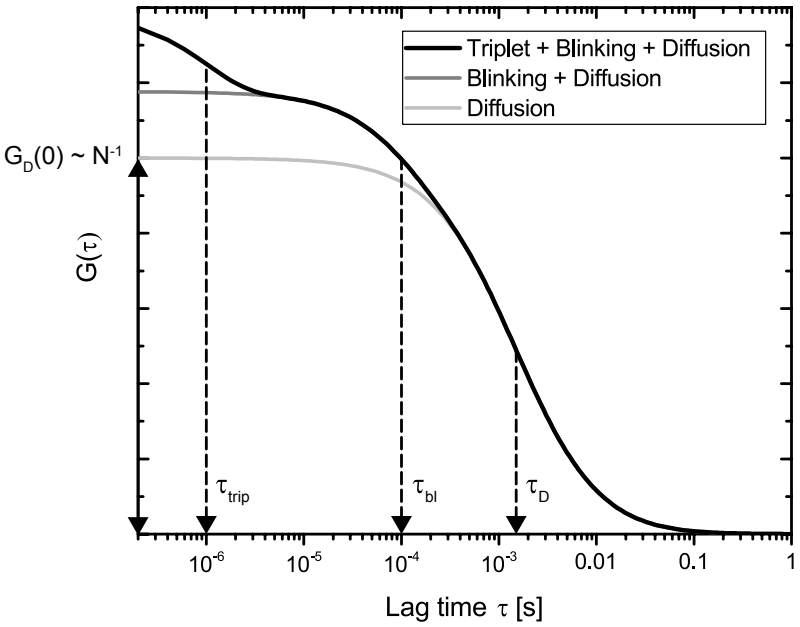


**Figure 2.3.: Simulation showing the effect of transient dark states on correlation functions.**
Numerical correlation function for a fluorophore with two non-radiative processes with characteristic relaxation times $\tau_{\mathrm{trip}}$ (triplet) and $\tau_{\mathrm{blink}}$ (blinking) as well as 3D diffusion through the focal volume.

$$G(\tau) = G_{\mathrm{D}}(\tau) \cdot G_{\mathrm{T_{trp}}}(\tau) \cdot G_{\mathrm{T_{bl}}}(\tau) \tag{2.13}$$

$$G(\tau) = \frac{1}{n}\left(1+\frac{\tau}{\tau_D}\right)^{-1}\left(1+\frac{\tau}{\mathrm{SP}^2\cdot\tau_D}\right)^{-1/2}\left(1+\frac{T_{\mathrm{trp}}}{1-T_{\mathrm{trp}}}\mathrm{e}^{-\tau/\tau_{\mathrm{trp}}}\right)\left(1+\frac{T_{\mathrm{bl}}}{1-T_{\mathrm{bl}}}\mathrm{e}^{-\tau/\tau_{\mathrm{bl}}}\right) \tag{2.14}$$

Fitting of measured correlation curves was performed with the program PyCorrFit v0.9.8 (Müller, Schwille and Weidemann, 2014) , using the Levenberg-Marquardt algorithm to minimize the sum of the squares. The structural parameter SP was fixed to 5 in all fitting procedures.

### Correcting for Non-Correlating Background

Non-correlating background $B$ contained in the fluorescent signal $S$ was accounted for by correcting the measured amplitude of the diffusional part $G_{\mathrm{D,meas}}(0)$ of the correlation function according to

$$G_{\mathrm{D,cor}}(0) = G_{\mathrm{D,meas}}(0)\left(\frac{S_1}{S_1-B_1}\right)\left(\frac{S_2}{S_2-B_2}\right), \tag{2.15}$$

where $S_1$ and $S_2$ are the average intensities detected in each channel of the used pseudo-cross-correlating setup. $B_1$ and $B_2$ are the corresponding background intensities determined by measurements of the fluorescence signal from plain potassium

phosphate buffer solutions, averaged over an acquisition time of 30 s for each individual laser power.

### Calculation of Laser Power Densities

The laser power density in the focal spot was calculated from the measured mean power $P$ of the laser beam and the beam diameter $\omega_0$:

$$I_0 = \frac{2P_0}{\pi\omega_0^2}. \tag{2.16}$$

The mean power $P_0$ was measured with a microscope slide power sensor (S170C, Thorlabs) after the excitation light passed the objective. The beam waist $w_0$ was determined by a calibration measurement with the synthetic dye ATTO 488 (ATTOTEC). From the diffusion time $\tau_D$ of ATTO488 measured at low excitation power ($\approx$0.2 kW/cm$^2$), one can estimate the beam waist $\omega_0$ by inserting the published diffusion coefficient ($D = 400\,\mu m^2/s$; Kapusta, 2010) into equation 2.8.

### Molecular Brightness (CPP)

One key parameter of all fluorescent dyes is their molecular brightness, stating how many photons per second per molecule a specific chromophore is able to emit. Making use of fluorescence correlation spectroscopy (FCS) one is able to access this quantity, also termed counts per particle (CPP) or counts per molecule (CPM). It is defined as CPP= $\langle F\rangle/\langle N\rangle$ with the mean fluorescence intensity $\langle F\rangle$ detected in counts per second and the mean number of molecules $\langle N\rangle$ in the detection volume.
As this parameter depends on excitation intensity, FCS measurements were performed over a broad range of laser irradiances to quantify the respective brightness of mNeonGreen, EGFP and AcGFP.

### Molecular Brightness (CPP) of oligomerized FPs

Special care has to be taken when the observed sample contains a mixture of fluorescent species. If the individual species have identical (or similar) diffusion times and only differ in their respective brightness, the amplitude of the correlation function is weighted proportionally to the square of the respective molecular brightness. For the CPP in a chain with binomially distributed non-fluorescent domains follows (Petrov and Schwille, 2008):

$$\begin{aligned}\psi_{\mathrm{cor}}(n) =& F(n)\, G_{\mathrm{D}}(0)\, \frac{\left(\sum_{i=1}^{n} \psi_i p_i\right)^2}{\sum_{i=1}^{n} \psi_i^2 p_i} \\ =& F(n)\, G_{\mathrm{D}}(0)\, \frac{\left(\sum_{i=1}^{n} i p_i\right)^2}{\sum_{i=1}^{n} i^2 p_i} \\ \overset{\substack{\mathrm{i}\geq 2 \\ \mathrm{p}<1}}{=}& F(n)\, G_{\mathrm{D}}(0)\, \frac{np}{np+1-p}\end{aligned} \tag{2.17}$$

CPP per fluorescent subunit in a FP n-mer:

$$\psi^1_{\mathrm{cor}}(n) = \frac{\psi_{\mathrm{cor}}(n)}{n_{\mathrm{eff}}(n)} = \frac{\psi_{\mathrm{cor}}(n)}{np+1-p} \tag{2.18}$$

$$= F(n)\, G_{\mathrm{D}}(0)\, \frac{np}{(np+1-p)^2} \tag{2.19}$$

Average number of fluorescent subunits in a FP n-mer as observed in an FCS experiment (multimers with zero fluorescent subunits are excluded):

$$n_{\mathrm{eff}}(n) = \frac{\sum_{i=1}^{n} \psi_i^2 p_i}{\sum_{i=1}^{n} \psi_i p_i}, \quad p_i = \binom{n}{i} p^i (1-p)^{n-i}, \quad i > 0 \tag{2.20}$$

$$= np + 1 - p \tag{2.21}$$

Using the probability of mNeonGreen to adopt a matured, fluorescent state ($p$ = 0.76%), the effective number of fluorescent domains in multimeric construct can be calculated:

| | $p = 76\,\%$ | | |
|---|---|---|---|
| $n$ | $n_{\mathrm{eff}}$ | $np/(np+1-p)$ | $np/(np+1-p)^2$ |
| 1 | 1 | (1) | (1) |
| 2 | 1.76 | 0.86 | 0.49 |
| 3 | 2.52 | 0.90 | 0.36 |
| 4 | 3.28 | 0.93 | 0.28 |
| 5 | 4.04 | 0.94 | 0.23 |

**Table 2.1.:** Effect of binomially distributed dark domains on CPP-values in tandem proteins.

## 2.3. Total Internal Reflection Fluorescence (TIRF) Microscopy

The single-molecule sensitivity of a total internal reflection fluorescence microscope (TIRFM) is achieved by its highly confined excitation volume, which is comparable

in size to a diffraction-limited spot in FCS. The spatial selectivity is accomplished by an evanescent field, which is generated by total internal reflection of an incident laser beam at the interface between a dense (usually glass) and a less dense medium (usually aqueous solutions) with refractive indices of $n_1$ and $n_2$, respectively. The excitation intensity $I_{\text{ex}}$ of the evanescent field decreases exponentially along the optical axis $z$:

$$I_{\text{ex}}(z) = I_0 \exp\left(-\frac{z}{d}\right). \tag{2.22}$$

The characteristic penetration depth $d$ at which the intensity of the evanescent field has dropped to $1/e$ of the peak intensity, can be estimated by (Gingell, Heavens and Mellor, 1987):

$$d = \frac{\lambda}{4\pi\sqrt{n_1^2 \sin^2\theta - n_2^2}}. \tag{2.23}$$

### 2.3.1. Single-Molecule Imaging

An inverted microscope (Axio.Observer Z1, Carl Zeiss AG) served as the body for the objective-based TIRF setup used in this study. The microscope was equipped with an oil immersion objective (100x/NA 1.46, Carl Zeiss AG) for high collection efficiency. GFP was excited with argon ion laser operating at 488 nm, and the fluorescence signal was detected by an EMCCD camera (Evolve 512, Photometrics) with an EM gain set to 1000. The laser power for imaging (≈25 mW) was adjusted in a way that for the mNeonGreen pentamer none of the pixels showed saturation. This power was then kept constant for all other constructs.

To be able to identify single molecules adsorbed on the glass surface, the GFP stock solutions were highly diluted to concentrations of approximately 50 pM into PBS pH7.5 and incubated 5 min on freshly plasma cleaned 8-well cover slide chambers (Eppendorf AG). After thorough washing with PBS the coverglass was imaged in TIRF mode using an oil immersion objective (100x / NA 1.46, Carl Zeiss) with a 1.6x post-magnification lens, giving a total magnification of 1600-fold. After quickly adjusting the focus at low laser power (4 mW), the movie was started with 20 frames per second until 750 images were acquired. 5-10 movies were recorded for each construct and saved as 16-bit image stacks.

### 2.3.2. Data Analysis

#### Image Processing

Using ImageJ, the initial frame of each movie was masked by a pixel threshold to discriminate between fluorescence signal ($\geq 2500$ camera count numbers) and background ($< 2500$ camera count numbers). This mask was then kept fixed throughout the movie and the average intensity of the fluorescence signal was plotted versus time. The threshold was chosen empirically so that it is considerably above the background to mainly detect the GFP fluorescence. As a control, different thresholding values were also tested without any effect on the results.

#### Criteria for spot selection from the movies

When performing single-molecule experiments of immobilized molecules adsorbed on a glass surface, special care has to be taken in discriminating between spots containing one fluorescent molecule and spots where two or more fluorophores or fluorescent contaminants are aggregated and not distinguishable due to the diffraction limited resolution. Using a self-written ImageJ plugin[i], this problem was addressed as reported previously (Ulbrich and Isacoff, 2007), by fitting a 2D elliptical Gaussian to the spot in each frame and plotting the corresponding angle of the fitted major axis to an arbitrary reference axis. If the point represents the PSF of a single fluorophore, one expects the angle to scatter randomly across the frames until the fluorophore bleaches, as well as a rather circular shape of the 2D gaussian (i.e. small eccentricity). If the bright spot would originate from aggregated fluorophores, the angle of the Gaussian fit is more stable due to a preferential orientation and a pronounced eccentricity of the spot. With this additional information one is able to quickly identify invalid spots, which reduces experimental bias in the single-molecule analysis.

## 2.4. Fluorescence Lifetime Measurements

The fluorescence lifetime measurements were performed using a Leica TCS SP5 X confocal microscope equipped with a pulsed white light laser (WLL, 80 MHz repetition rate, NKT Photonics), a FLIM X16 TCSPC detector (LaVision Biotec) and a 63x water objective (HCX PL APO CS, NA 1.2). The detection covered a time window of 12.24 ns after the excitation pulse with a temporal resolution of 0.08 ns. A custom-written MATLAB script (Austen et al., 2015) extracted the photon counts for each time increment and region of interest. For *in vivo* measurements, the ROI was manually selected for single cells. For *in vivo* measurements, the photon counts were

[i] Armin Lambacher, Max Planck Institute of Biochemistry, Germany

summed up over the whole frame. The instrument response function of the setup was determined with a scattering solution (LUDOX, Sigma-Aldrich). By approximating the IRF with a Gaussian function, one is able to deconvolve the fluorescence lifetime analytically with the fitting function $F$:

$$
\begin{aligned}
f(t) &= \Theta(t-t_0)\, A \exp\left(-\frac{t-t_0}{\tau}\right), \quad \Theta(t)\text{: Heaviside step function} \\
g(t) &= \frac{1}{\sqrt{2\pi}\sigma} \exp\left(-\frac{t^2}{2\sigma^2}\right) \\
(f \otimes g)(t) + y_0 &= \int_{-\infty}^{\infty} f(\tau) g(t-\tau)\, \mathrm{d}\tau + y_0 \\
F(t) &= \frac{1}{2} A \exp\left(\frac{\sigma^2 - 2\tau(t+t_0)}{2\tau^2}\right)\left(1 - \mathrm{Erf}\left[\frac{\sigma^2 - \tau(t+t_0)}{\sqrt{2}\sigma\tau}\right]\right) + y_0
\end{aligned}
\tag{2.24}
$$

The convolution integral was evaluated using *Mathematica 10.1* (Wolfram Research, USA).

## 2.5. Preparation and Purification of mNeonGreen Oligomers

The fluorescent proteins used in solution studies were provided by Magnus-Carsten Huppertz, Max Planck Institute of Biochemistry.
mNeonGreen (1x – 5x) are multimeric fluorescent proteins, with 5-amino-acid (E-G-A-G-A) linkers connecting individual mNeonGreen units. We inserted the mNeonGreen gene (AlleleBiotech) into the NotI restriction site of a pET-28a(+) vector (Clonetech) to obtain a C-terminal His6-tagged fragment. Next, we transferred mNeonGreen-His6 into the NotI restriction site of the pEGFP-N1 vector (Clonetech). We digested vector backbones with BsrGI and mNeonGreen inserts with BsrG1 and Not1 to clone tandem mNeonGreen expression constructs containing a C-terminal His6-tag. To confirm sequences of mNeonGreen expression constructs, we first digested respective plasmid DNA with the restriction enzymes NotI and BamHI to yield expected lengths for mNeonGreen tandem inserts (see fig. 2.4a). All plasmid constructs were send for sequencing (Eurofins Genomics) with corresponding sequencing primers (see sequence alignment in fig. 2.5).
HEK293T cells were seeded 72 h before harvesting in T-75 flasks ($1.5 \cdot 10^6$/18 mL) and cultivated in DMEM containing 10% fetal calf serum in humidified 5% $CO_2$ atmosphere at 37 °C. Cells were transfected with 10 µg mNeonGreen vector according to TurboFect Transfrection Reagent Instructions (Thermo Scientific). Transiently transfected cells were briefly washed with 1x PBS and harvested by scraping cells from the dish while applying ice-cold lysis-buffer (1x PBS/cOmplete ULTRA protease

inhibitor/10 mM imidazole) to cells. Harvested cells were collected by centrifugation at 1000 × g and 4 °C for 30 min. Supernatants were discarded and pellets were resuspended in 1 mL lysis buffer containing 1 µL Benzonase nuclease (250 U/µL). Cells were subsequently lysed by sonication (10 sec pulse, 30 sec break, 6 times, 10% power) and centrifuged at 20 000 × g and 4 °C for 30 min to separate protein bearing supernatants from cell debris. His6-tagged mNeonGreen proteins were purified on 1 mL Ni-NTA superflow beads (Qiagen). The column was washed three times with 10 mL lysis buffer. Proteins were eluted with elution buffer (1x PBS, cOmplete ULTRA protease inhibitor, 250 mM imidazole). Eluates were dialyzed against 1x PBS buffer (pH 7.5) at 4 °C, overnight. Proteins were stored in 1x PBS at 4 °C until further use. Purified proteins were separated by SDS-PAGE to assure purity and full-length expression of mNeonGreen oligomers (see fig. 2.4b). The double band visible in SDS-PAGE of monomeric mNeonGreen is an artifact caused by boiling to denaturate the proteins (see fig. 2.4c).In addition, the fluoroscence of each oligomer was visualized by in-gel analysis see (fig. 2.4d).

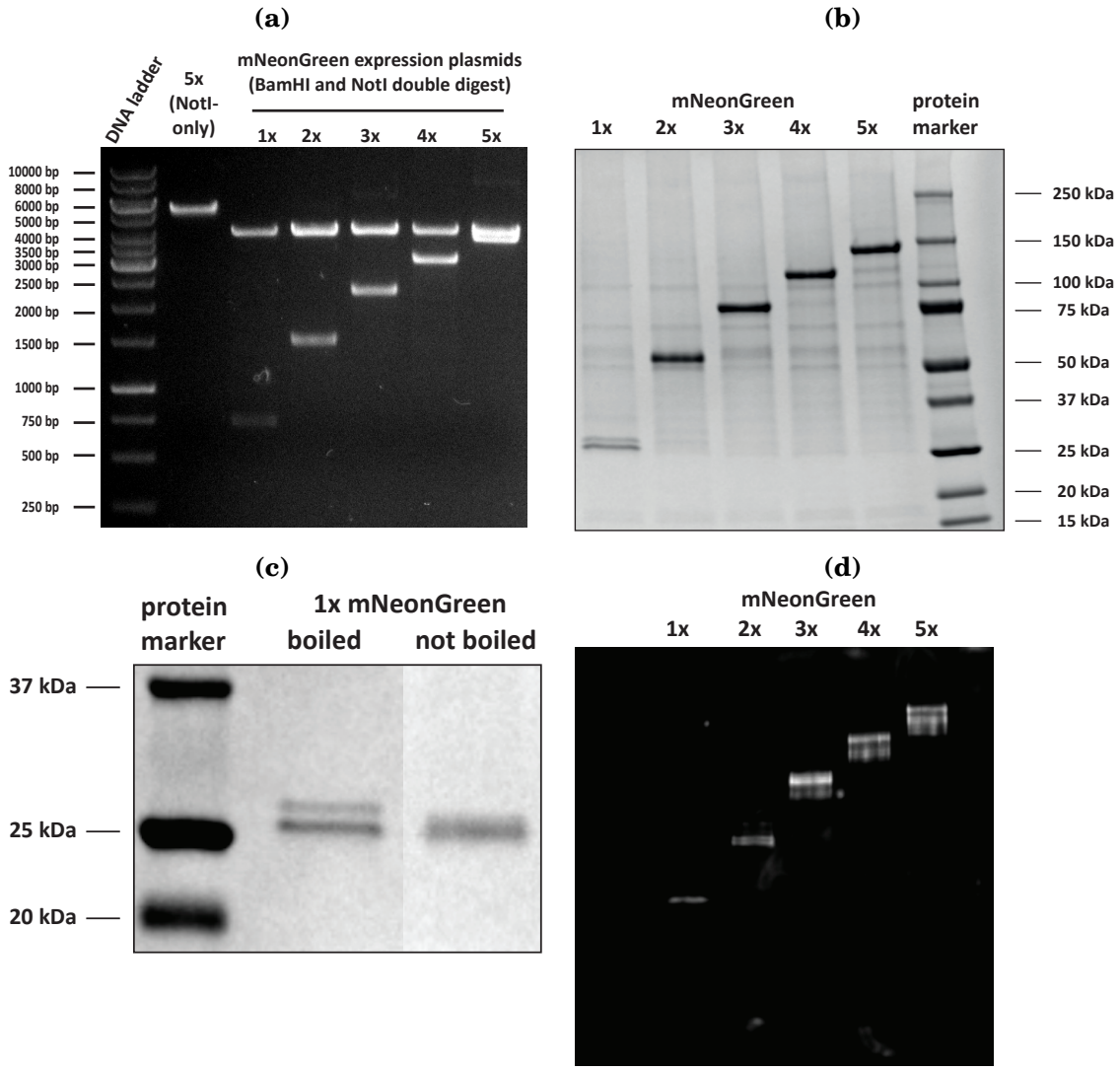


**Figure 2.4.: Gel electrophoresis of mNeonGreen DNA fragments and purified mNeonGreen oligomers.**
(a) Expression vectors of mNeonGreen oligomers were digested with BamHI and NotI at 37°C for 1h followed by an inactivation step at 80°C for 10 min. Samples were mixed with 6x DNA loading dye and separated on a 1% agarose gel (containing SYBR Safe DNA stain) in 1x TAE buffer at 100 V for 1h.
(b) Denaturating 4-20% SDS-gel (BioRad) of mNeonGreen oligomers. HEK293T cells were lyzed by sonication, centrifuged and supernatants were purified with Ni-NTA super flow columns. Proteins were separated in 1x Elpho buffer with 60 A for 30 min and stained with Coomassie brilliant blue solution. The gel was recorded as 16-bit grey scale images.
(c) Denaturating 4-20% SDS-gel (BioRad) of mNeonGreen monomers. Purified mNeonGreen monomers were mixed with 1x Laemmli sample buffer containing beta-mercapto ethanol and were either boiled at 95°C for 10 min or kept on RT. Proteins were separated according to (b).
(d) Native polyarcryl amide gel of mNeonGreen visualized with a Abrasham A600 scanner. The in-gel fluorescence of mNeonGreen oligomers was visualized using a LED emitting at 488 nm for excitation and was detected using pre-installed corresponding filter settings on a CCD camera. Figures kindly provided by Magnus-Carsten Huppertz.

**(a)**

```
91.6% identity in 250 residues overlap; Score: 1254.0; Gap frequency: 0.0%

EGFP-H6          1 MVSKGEELFTGVVPILVELDGDVNGHKFSVSGEGEGDATYGKLTLKFICTTGKLPVPWPT
AcGFP-H6         1 MVSKGAELFTGIVPILIELNGDVNGHKFSVSGEGEGDATYGKLTLKFICTTGKLPVPWPT
                   ***** ***** **** ** ****************************************

EGFP-H6         61 LVTTLTYGVQCFSRYPDHMKQHDFFKSAMPEGYVQERTIFFKDDGNYKTRAEVKFEGDTL
AcGFP-H6        61 LVTTLSYGVQCFSRYPDHMKQHDFFKSAMPEGYIQERTIFFEDDGNYKSRAEVKFEGDTL
                   *****  ************************** ******* ****** ***********

EGFP-H6        121 VNRIELKGIDFKEDGNILGHKLEYNYNSHNVYIMADKQKNGIKVNFKIRHNIEDGSVQLA
AcGFP-H6       121 VNRIELTGTDFKEDGNILGNKMEYNYNAHNVYIMTDKAKNGIKVNFKIRHNIEDGSVQLA
                   ****** * ********** * ***** ****** ** **********************

EGFP-H6        181 DHYQQNTPIGDGPVLLPDNHYLSTQSALSKDPNEKRDHMVLLEFVTAAGITLGMDELYKA
AcGFP-H6       181 DHYQQNTPIGDGPVLLPDNHYLSTQSALSKDPNEKRDHMIYFGFVTAAAITHGMDELYKA
                   ************************************    ***** ** ********

EGFP-H6        241 AALEHHHHHH
AcGFP-H6       241 AALEHHHHHH
                   **********
```

**(b)**

```
27.0% identity in 252 residues overlap; Score: 165.0; Gap frequency: 2.8%

EGFP-H6          1 MVSKGEELFTGVVPILVELD--GDVNGHKFSVSGEGEGDATYGKLTLKFICTTGKLPVPW
mNG-H6           1 MVSKGEEDNMASLPATHELHIFGSINGVDFDMVGQGTGNPNDGYEELNLKSTKGDLQFSP
                   *******      *   **   *  **  *   * * *    *   *    * * *

EGFP-H6         59 PTLVTTLTYGVQCFSRYPDHMKQHDFFKSAMPEGYVQERTIFFKDDGNYKTRAEVKFEGD
mNG-H6          61 WILVPHIGYGFHQYLPYPDGMSPFQA-AMVDGSGYQVHRTMQFEDGASLTVNYRYTYEGS
                     **     **       *** *           **   **  * *           **

EGFP-H6        119 TLVNRIELKGIDFKEDGNILGHKLEYNYNSHNVYIMADKQKNGIKVNFKIRHNIEDGSVQ
mNG-H6         120 HIKGEAQVKGTGFPADGPVMTNSL----TAADWCRSKKTYPNDKTIISTFKWSYTTGNGK
                         **  *  **       *                 *               *

EGFP-H6        179 LADHYQQNTPIGDGPVLLPDNHYLSTQSALSKDPNEKRDHMVLLEFVTAAGITLGMDELY
mNG-H6         176 RYRSTARTTYTFAKPMAANYLKNQPMYVFRKTELKHSKTELNFKEWQKAFTDVMGMDELY
                         *     *                                 *   *     ******

EGFP-H6        239 KAAALEHHHHHH
mNG-H6         236 KAAALEHHHHHH
                   *************
```

**Figure 2.5.: Sequence alignment of the characterized monomeric GFP variants.** AcGFP (a) and mNeonGreen (b) were aligned against EGFP using the SIM alignment tool (Expasy). The amino acids forming the hydroxybenzene-imidazolinone chromophore are highlighted (red box), as well as the hexahistidine affinity tag at the C-terminus that was used for purification (black box). Note that the first 7 N-terminal amino acids of mNeonGreen were derived from EGFP (6 amino acids from wtGFP plus an additional V inserted at position 2).

# 3. Steady-State Fluorescence Spectra of GFP constructs

Absorption and emission spectra were recorded with a Jasco V-650 spectrophotometer and a Jasco FP-8500 fluorospectrometer. GFP samples were measured in stock solution at about 500 nM (absorption) or diluted to 15 nM in PBS pH 7.5 (fluorescence emission).

Compared to EGFP, mNeonGreen is slightly red-shifted both in excitation and emission, while AcGFP is blue-shifted. The excitation peaks are positioned at wavelengths 477 nm for AcGFP, 489 nm for EGFP and 505 nm for mNeonGreen, the emission peaks at wavelengths 505 nm for AcGFP, 511 nm for EGFP and 518 nm for mNeonGreen. Further studies on the photophysical properties of the three GFP variants were performed using argon ion lasers operating at 488 nm. When comparing the respective brightess of the GFP variants, it has to be taken into account that excitation of 488 nm matches with the absorption peak of EGFP (100 %), but is less efficient for AcGFP (84 %) and especially for mNeonGreen (59 %).

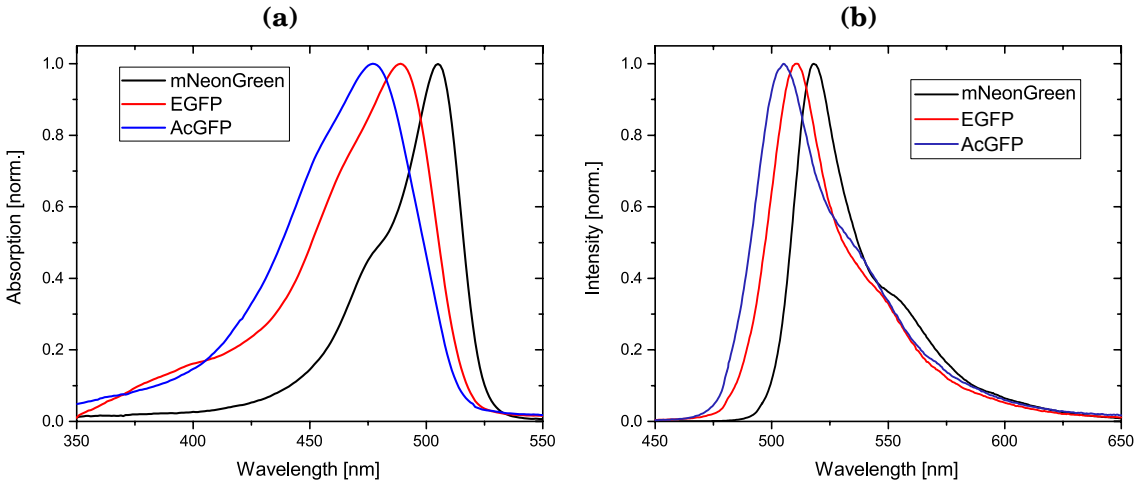


**Figure 3.1.: Absorption and emission spectra of mNeonGreen, EGFP and AcGFP.** (a) Absorption spectra were recorded at a scan speed of 400 nm/min and with a bandwith of 1 nm. Spectra were corrected for Rayleigh scattering. (b) Emission spectra were recorded at a scan speed of 50 nm/min and with slit widths of 5 nm for excitation and emission. Compared to EGFP, AcGFP is blue-shifted, while mNeonGreen is red-shifted, in both absorption and emission.

# 4. TIRF Microscopy of Immobilized GFPs

Total internal reflection fluorescence (TIRF) microscopy provides the possibility to excite only fluorophores that are located near a solid surface. The hereby achieved high spatial selectivity suppresses fluorescent contributions from fluorophores or autofluorescent contaminants in layers above and facilitates the detection of fluorescence down to a single-molecule level. This unique feature was exploited to visualize single photobleaching events of monomeric mNeonGreen and mNeonGreen tandem with up to five domains. Photobleaching statistics is used to estimate the probability of mNeonGreen to be inherently non-fluorescent due to misfolding or unsuccessful maturation. This quantity can be of importance when using mNeonGreen as a protein tag or when addressing the stoichiometry of complexes in single-molecule bleaching assays. Additionally, bleaching times of mNeonGreen, EGFP and AcGFP monomers are determined by single-molecule lifetime distributions and compared to bulk photobleaching rates from ensemble measurements.
Diffraction-limited spots representing individual molecules of mNeonGreen, EGFP and AcGFP are shown in fig. 4.1. All images were recorded at the same illumination power and identically post-processed using ImageJ. Therefore, the individual spots reflect the brightness of the single molecules given that the proteins have no tendency to dimerize or aggregate. The data show that mNeonGreen is considerably brighter than EGFP and AcGFP.

## 4.1. Photostability of mNeonGreen, EGFP and AcGFP

For practically all applications in fluorescence microscopy and fluorescence spectroscopy it is crucial to estimate of the absolute or relative photostability of the fluorescent dyes. To compare the photostability between the three GFP variant, the bleaching kinetics was determined by two complementary approaches. First, the total fluorescence signal averaged over the whole image frame was monitored as a function of time to extract the bulk photobleaching rate. Second, the lifetime before photobleaching of individual molecules identified in the TIRF movies was measured with statistically analyzed.
First, the bleaching rate of mNeonGreen, EGFP and AcGFP was determined in bulk

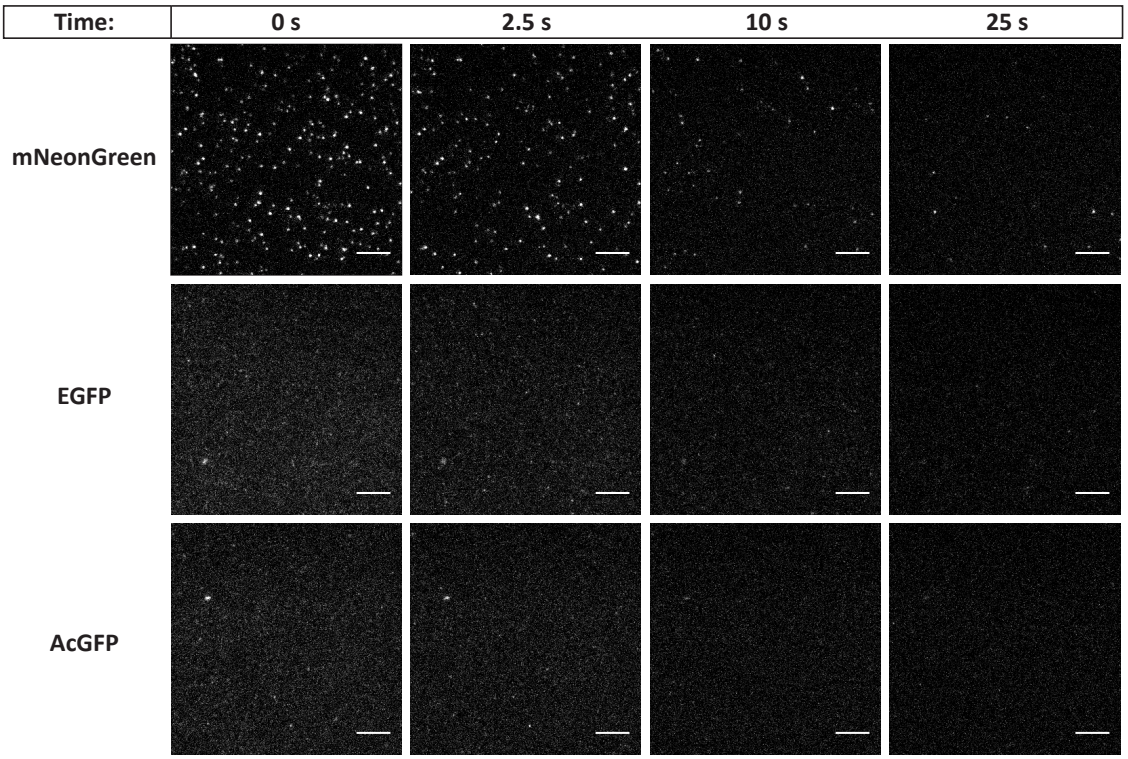


**Figure 4.1.: mNeonGreen is clearly superior in brightness compared to EGFP and AcGFP in single-molecule TIRFM.**
Representative TIRF images showing mNeonGreen, EGFP and AcGFP adsorbed on glass in TIRFM 0 s, 2.5 s, 10 s and 25 s after laser activation. Each 16-bit image was post-processed in the same manner for illustration using ImageJ: The minimum displayed value in the gray is equivalent to 71 camera count numbers, maximum displayed value is equivalent to 3736 camera count numbers, corresponding to 0.35 % saturated pixels in the initial ($t = 0$ s) frame showing mNeonGreen. Scalebars 5 µm.

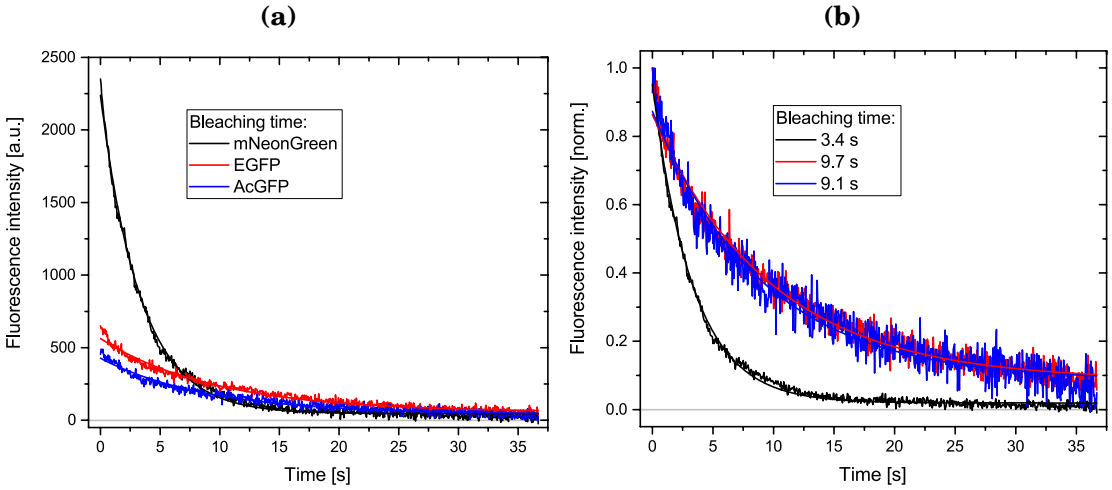


**Figure 4.2.: Bulk fluorescence decay of mNeonGreen, EGFP and AcGFP as seen in TIRFM movies.**
Fluorescence from spots detected in each frame masked by pixel value thresholding was averaged and plotted versus time for mNeonGreen, EGFP and AcGFP (a). The individual decays are adequately fitted by single exponential with characteristic bleaching times of $(3.4 \pm 0.1)$ s for mNeonGreen, $(9.7 \pm 0.2)$ s for EGFP and $(9.2 \pm 0.2)$ s for EGFP. Normalization of each curve to the initial amplitude illustrates the relative bleaching kinetics, showing that EGFP and AcGFP are almost 3 times more photostable compared to mNeonGreen at the laser power (25 mW) tested.

to access information about the relative photostability of the three variants.

Using ImageJ, the initial frame of each movie was masked by a pixel threshold to discriminate between fluorescence signal and background (see methods 2.3.2). This mask was then kept fixed throughout the movie and the average intensity of the fluorescence signal was plotted versus time (see fig. 4.2a). The result confirms the observation already made from the images in figure 4.1 and shows that the average fluorescence intensity of mNeonGreen is about 3 times higher compared to EGFP and AcGFP. However, a fit of the intensity decay to an exponential function of type $F = A \exp -\kappa t$ showed that mNeonGreen also bleaches roughly 3 times faster than EGFP and AcGFP under the conditions tested. The sensitivity of mNeonGreen to photodestruction is emphasized in fig. 4.2b, which shows the respective intensity traces normalized to the initial amplitude. The photobleaching rates were determined to $(0.29 \pm 0.01)\,s^{-1}$ for mNeonGreen, $(0.10 \pm 0.01)\,s^{-1}$ for EGFP and $(0.11 \pm 0.01)\,s^{-1}$ for AcGFP. The values are the mean ± s.d. from five movies for each construct.

For this purpose, the lifetime before photobleaching was determined for a large number of single molecules and plotted in a histogram. The result for monomeric ($n = 207$ spots) and trimeric mNeonGreen ($n = 240$ spots) can be seen in figure 4.3. Fitting the histogram to an exponential decay function of the type $F = A \exp(-\kappa t)$ yielded bleach-

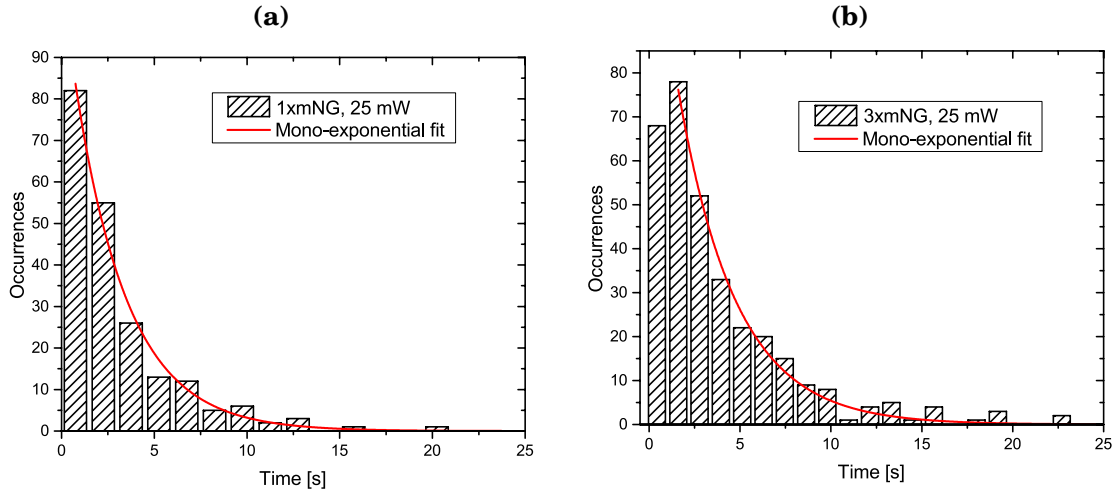


**Figure 4.3.: Single fluorophore lifetime distribution before photobleaching of mNeonGreen.**
Histograms showing the fluorescent time-span of single fluorophores for monomeric mNeonGreen (207 spots) and trimeric mNeonGreen (240 spots, 487 individual bleaching events) at the same laser power. These were fitted to mono-exponential decays with characteristic bleaching times of $(2.8 \pm 0.1)$ s for 1xmNeonGreen and $(3.2 \pm 0.1)$ s for 3xmNeonGreen, consistent with the results from bulk experiments. Binsize of the individual histograms had no effect on the results and was set according to the Freedman-Diaconis rule to (a) 1.5 s and (b) 1.15 s.

ing times $\kappa_{1x} = (0.36 \pm 0.01)\text{s}^{-1}$ for monomeric and $\kappa_{3x} = (0.31 \pm 0.01)\text{s}^{-1}$ for trimeric mNeonGreen.

## 4.2. Non-Fluorescent Fractions of mNeonGreen

The intensity trajectoy of bright spots in the first frame after laser activation was plotted using an ImageJ plugin.

To evaluate the number of fluorescent domains per molecule, bleach steps in trajectories of individual molecules were statistically analyzed in time-lapsed image stacks (fig. 4.4). For the mNeonGreen trimer (3xmNeonGreen), over 500 spots from six different locations on the coverglass were analyzed and classified into the number of observable distinct bleaching steps (1, 2 and 3 steps) or discarded as invalid (e.g. due to aggregated proteins, weakly fluorescent contaminants, or movement of the spot during the movie). From 557 analyzed spots of 3xmNG, 240 fulfilled the criteria (see section 2.3.2) to be processed as single-molecule data and were categorized into the number of observed bleaching steps. In fig. 4.5a, the red columns represent a binomial fit to the data which yields an estimated probability for the fluorophore to be fluoerescent in this case 68 %.

The distribution of observed bleaching steps is broadened for two reasons: Firstly,

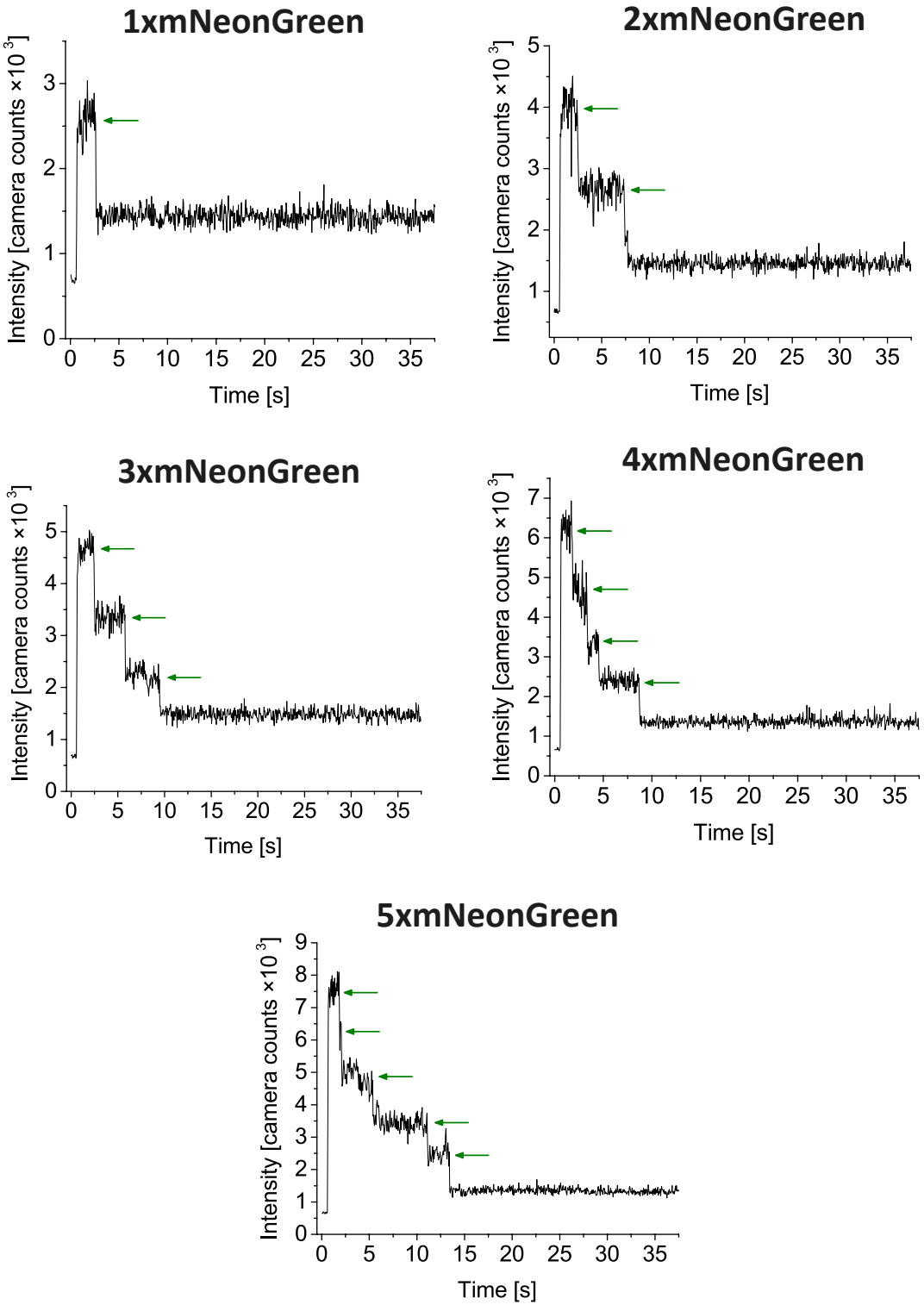


**Figure 4.4.: Representative time traces of fluorescence emission of mNeonGreen oligomers recorded in TIRFM show typical quantitized photobleaching events.**
Irreversible photobleaching of single fluorophores can be seen by distinct drops of intensity in the fluorescence trajectories, occuring at the times indicated by green arrowheads.

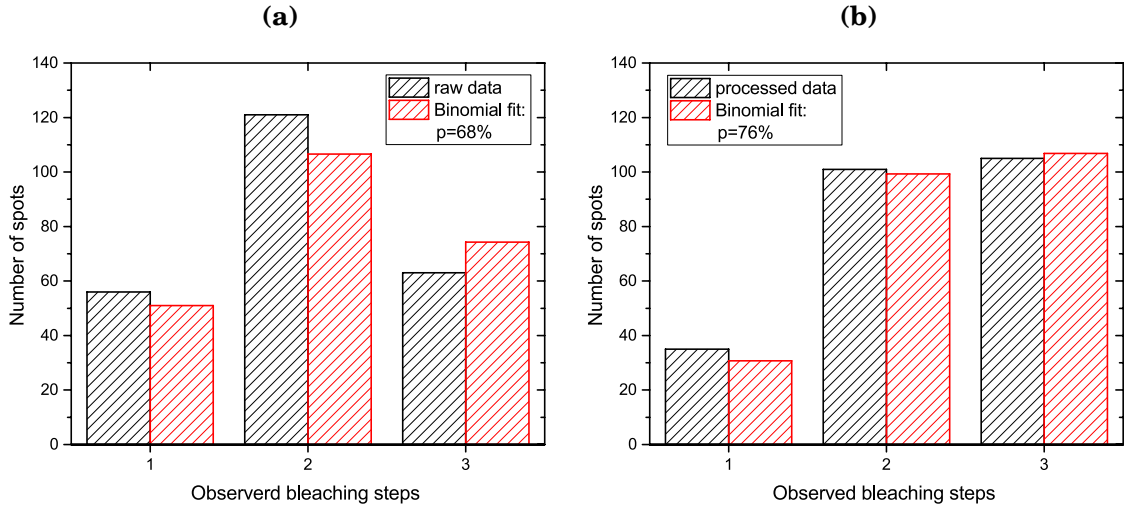


**Figure 4.5.: Distribution of number of steps observed in mNeonGreen single-molecule photobleaching analysis.**
(a) Histogram showing the number of bleaching steps observed for each individual spot (240) (black columns) together with a binomial fit to the data (red columns), assuming that the distribution of step counts is caused mainly by randomly non-fluorescent subunits present in each trimer. (b) Taking into account that single bleaching steps are not detected when they coincide within the time scale of the camera acquisition rate, a binomial distribution fit to the data corrected for missed events gives an estimate of $(76 \pm 2)\,\%$ for the probability that a single mNeonGreen protein is fluorescent.

due to the definite time resolution of the camera (integration time of 50 ms), there is a certain probability that two or more individual bleaching steps fall into such a small time interval so that it is not possible to identify the bleaching step as in fact two or more distinct bleaching steps in the time trace. Secondly, GFPs have a certain probability of beeing mis-folded or non-correctly matured, leading to non-fluorescent domains.

To account for possibly missed bleaching events, the distribution of observed intensity amplitudes from individual steps is analyzed (see fig. 4.6b). Since the step height of a missed event will be roughly double as much as the one of a single bleaching step, the number of steps with a height larger than that of a typical monomeric bleaching event should be indicative of the number of missed events during the analysis. For this purpose, the step height distribution of the 1xmNG is shown as a reference (fig. 4.6a). Comparing both distribution, one can see that the dominant peak of 3xmNeonGreen matches with the distribution of 1xmNeonGreen. Therefore, a single mNeonGreen fluorophore has, under these conditions, an average fluorescence intensity of about 1100 camera counts. Additionally, the center $x_c$ of the fitted peak 2 and peak 3 rise linearly as one would expect for a simultaneous double and triple bleaching event, respectively. The area of the histograms represent the fraction of molecules undergoing

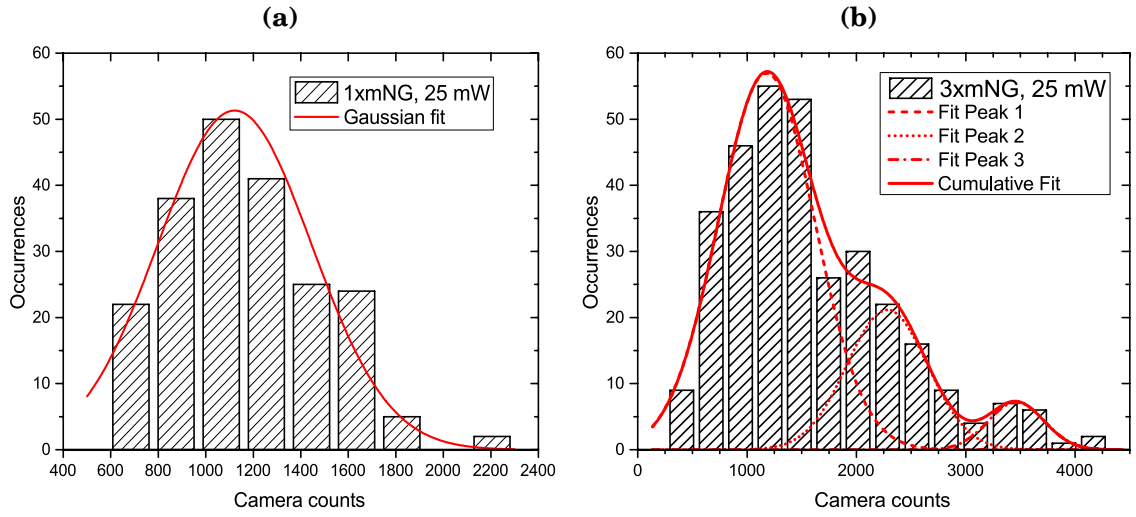


**Figure 4.6.: Distribution of step-wise intensity drops of monomeric and trimeric mNeonGreen detected in single-molecule photobleaching analysis.** Histograms showing the average amplitude of fluorescence intensity relative to the background intensity or relative to the next lower intensity plateau in cases where multiple steps are observed within a time trace. This analysis was done for monomeric mNeonGreen (a) and trimeric mNeonGreen (b) to quantitatively determine the relative step height of single mNeonGreen fluorphores which is proportional to the molecular brightness. The histogram corresponding to 1xmNeonGreen features a peak located at $1120 \pm 30$ (in camera count numbers), which is also present in the data of 3xmNeonGreen with a center at $1180 \pm 80$ as approximated by Gaussian fits. In addition, two smaller peaks shifted to higher count numbers can be identified whose centers are located at roughly 2 times ($2280 \pm 190$ and 3 times ($3460 \pm 210$ higher intensities compared to the predominant peak. This is caused by the simultaneous bleaching of two and three subunits within a trimer that can not be resolved as individual events and are thus treated as a single bleaching event. Based on the relative areas under each peak one can estimate a probability of 31 % and 7 % that a double and triple bleaching event is missed, respectively.

1, 2 or 3 simultaneous bleach steps within the selected ensemble. The ratio of area 2 with respect to area 1 (31 %) was used as a factor to correct for two coinciding bleaching events. Consistently the ratio of area 3 with respect to area 1 (7.3 %) was used as a factor for three simultaneous bleaching events. This transforms the distribution in figure 4.5a into that shown in 4.5b. A binomial fit to the adjusted distribution estimates a probability of $p = 76\%$ for a mNeonGreen protein to be fluorescent inside the trimeric chain.

# 5. Fluorescence Spectroscopy of Monomeric GFP Variants

Next, the photophysical properties of the three GFP variants mNeonGreen, EGFP and AcGFP were addressed in more detail using fluorescence correlation spectroscopy (FCS) and fluorescence lifetime measurements. This includes a detailed examination of the molecular brightness of each fluorescent protein over a broad range of laser powers, a characterization of non-radiative transient dark states as well as their sensitivity towards changes in pH of the surrounding solution.

## 5.1. Molecular Brightness of mNeonGreen, EGFP and AcGFP

### 5.1.1. Power Series in a Diffraction-Limited Focus Volume

By exploiting the full power range of the argon laser in the setup and setting the confocal pinhole to a diameter of 1 airy unit (= 34 µm), correlation curves of mNeonGreen, EGFP and AcGFP were recorded over a range from 0.1 kW/cm$^2$ to 800 kW/cm$^2$ with an acquisition time of 60 s. Each measurement was repeated 10 times in row.
The correlation curves were fitted with a T-T-3D model (see eq. 2.14) containing two contributions characteristic blinking times and a diffusion-related decay: one contribution accounts for singlet-triplet transitions typically taking place in the microsecond timerange (1 – 10 µs), while the other contribution describing the commonly observed protonation-dependent blinking of fluorescent proteins in the sub-millisecond timerange (10 – 300 µs).
The behavior of the CPP versus excitation intensity can be separated into three different regimes based on the underlying effects causing the progressivity:
At relatively low excitation intensities ranging from 0.1-2 kW/cm$^2$, the CPP of each GFP rises linearly with excitation power as expected for one-photon excitation. This proportionality of CPP to $I_0$ is confirmed by fitting the first three data points with a power law of type $ax^b$; the estimated exponents are close to 1 ($b$ = 1.04 for mNeonGreen, $b$ = 1.09 for EGFP, $b$ = 1.08 for AcGFP). In this regime, mNeonGreen is approximately 1.6 times brighter than EGFP and 2.9 times brighter than AcGFP.
As the power increases further, photophysical dynamics in the fluorophores start to

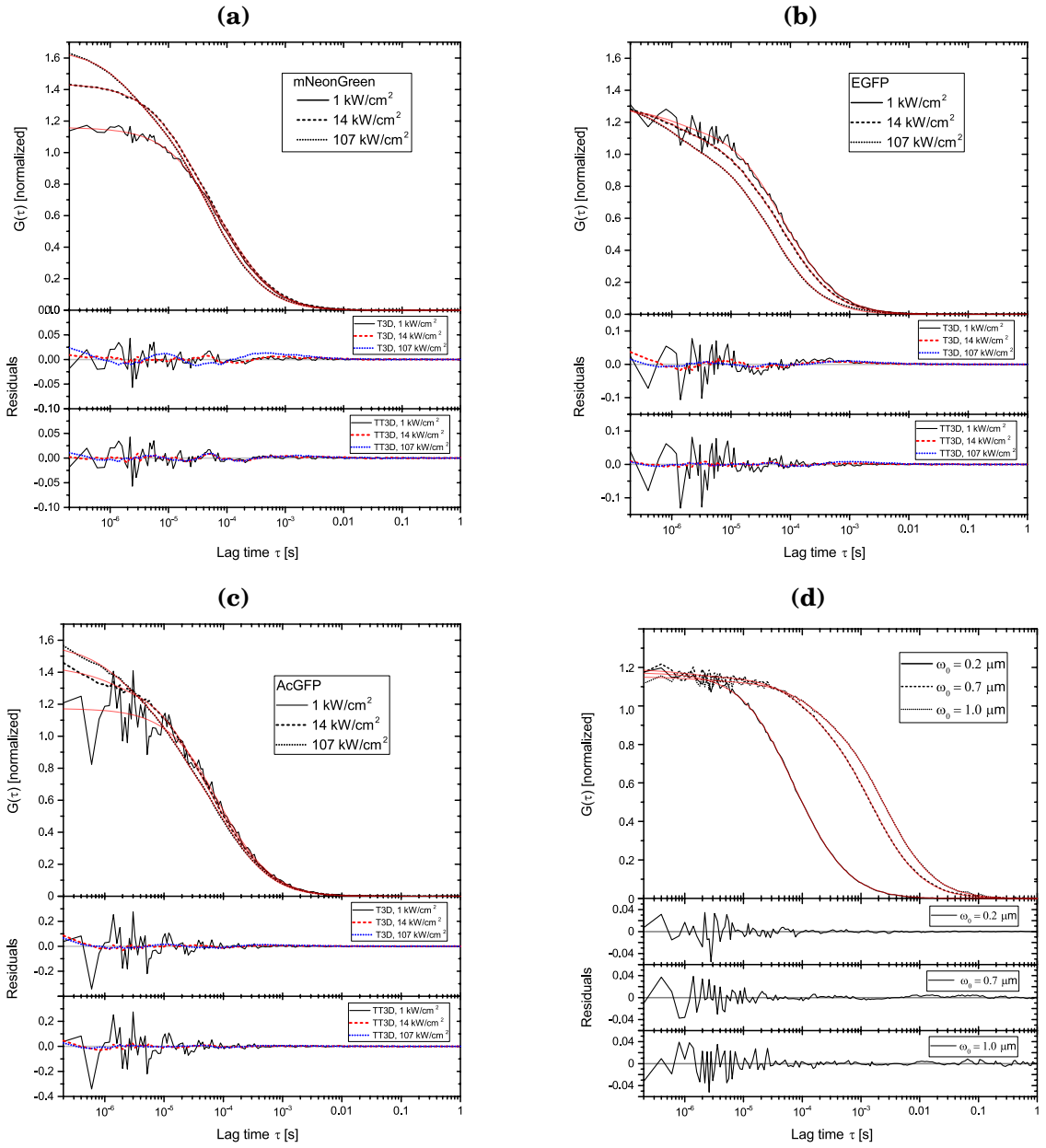


**Figure 5.1.: Effect of the excitation intensity and size of the observation volume on autocorrelation functions (ACFs) of mNeonGreen, EGFP and AcGFP.** Each ACF shown is the average of five measurements with an acquisition time of 60 s. Residuals show the fitting quality of two models tested which contain in one case two independent components (T3D), one singlet-triplet transition and one diffusion, and in the other case three components with two contributions from non-radiative relaxation (TT3D) instead of one. used to describe the data for a model containing two components (T3D) and three components (TT3D), the latter of which is superimposed on the correlation data (red lines).

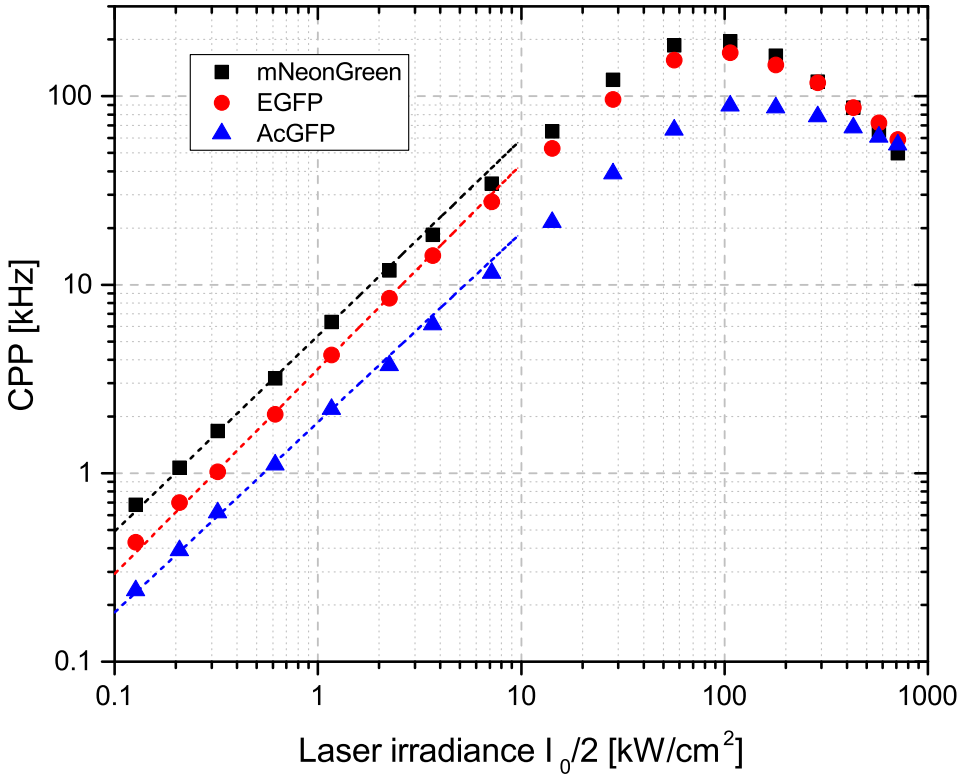


**Figure 5.2.: Molecular brightness of freely diffusing mNeonGreen, EGFP and AcGFP, as measured in FCS over a broad laser power range.**
Data is fitted to a power law of type $ax^b$ (dashed lines), yielding values for $b$ close to 1 as expected for a single-photon excitation process. The laser irradiance $I_0$ was estimated from the mean power of the laser beam $P$ and the beam waist $\omega_0 = 0.2\,\mu\text{m}$, determined by a reference measurement of ATTO488: $I_0 = 2P/(\pi\omega_0^2)$. $\lambda_{\text{exc}} = 488\,\text{nm}$, $T = 298\,\text{K}$, Setup used in the study: Zeiss LSM780 ConfoCor3.

rise and distort the proportionality and thus, the linear increase. A growing fraction of molecules is driven into the excited state leading to a depletion of fluoropohores in the excitable ground state. This saturation effect leads to a reduced photon yield which can be achieved per further irradiance boost, causing the CPP to drop at higher excitation intensities. This can be seen by deviations from the linear slope in the log-log plot at laser irradiances above 2 kW/cm$^2$. Above 10 kW/cm$^2$ the quenching of fluorescence emission per molecule is amplified by increased de-excitation of the excited state non-radiative triplet states via intersystem crossing. This can be seen by a stark rise of the triplet fraction contributing to the correlation functions of all three GFP variants.
At 100 kW/cm$^2$ of laser irradiance, the CPP reaches a maximum and starts to drop if the laser power is further increased. This can be explained by irreversible photobleaching of the fluorophores at the high irradiances applied. Due to the exponential nature of the bleaching process, with an inreasing photon influx, the average survival-time of the GFPs decreases with inreasing photon influx and will, at some point, drop below the residence time inside the focal volume. This leads to a significant fraction of fluorophores that bleach during their diffusion through the focal volume and thus, stop contributing to the fluorescence emission, leading to a drop in CPP.
During the fitting process it became clear that the recorded correlation curves are not well suited for a more detailed analysis of the power dependence of the individual correlation times governing the shape of the correlation function. The fast diffusion of the GFPs through the focal volume in 100 µs coincides with the relaxation time expected for protonation- or isomerization dependent blinking, making it impossible to discriminate between the individual processes.
To circumvent this problem, the focal volume was enlarged by underfilling the back-aperture of the objective which increased the waist $\omega_0$ of the detection volume by a factor of up to 5 (see fig. 5.1d). As a consequence, the diffusion time of the fluorophores prolongs by a factor of $5^2 = 25$ reaching time scales above 2 ms. This adjustment in the experimental design prevents the overlap of time regimes of transient states of the fluorophore with the residence time inside the focal volume and facilitates the separation of the distinct components in the autocorrelation function.

### 5.1.2. Power Series with an Enlarged Focus Volume

Now, correlation functions of the three GFP variants diluted to 5 nM were recorded using a 20% underfilled objective at identical buffer conditions (10 mM phosphate buffer pH 8). The measurement at each laser irradiance was repeated 15 times with an acquisition time of 30 s.

Due to constraints of the setup used in this study, underfilling reduced the applicable laser power range from 0.1 –700 kW/cm$^2$ as in the previous experiment to 0.1–2 kW/cm$^2$. This confines detailed photophysical analysis of the GFPs to the low to moderate irradiance regime, which however still covers the range of typical fluorescence microscopy and fluorescence spectroscopy experiments.
The measured correlation curves were fitted again with the T-T-3D model (see eq. 2.14) that accounts for singlet-triplet transitions and a second transient state attributed to isomerization or protonation processes in or near the chromophore, commonly termed as blinking.
Figure 5.3a shows the molecular brightness of the mNeonGreen, EGFP and AcGFP as a function of excitation intensity as calculated from FCS measurements in an enlarged focal volume. For the first three data points corresponding to irradiances of 0.1, 0.2 and 0.3 kW/cm$^2$, respectively, the fluorescence emission per molecule rises proportional to the laser power increase for all GFP variants. This is emphasized in fig. 5.3b that shows the respective brightness values normalized to the fitted CPP of EGFP. From 0.1 – 0.3 kW/cm$^2$, the CPP of each GFP remains constant within the experimental uncertainty indicated by the error bars (standard deviation of 15 measurements). With higher intensities, the relative photon yield decreases continuously. The relative CPP of each GFP when excited with 2.0 kW/cm$^2$ instead of 0.1 kW/cm$^2$ drops by 14 % for mNeonGreen, 10 % for EGFP and 19 % for AcGFP.
When comparing the progressivity of CPP with increasing laser irradiance between the three GFPs in the normalized plot, it seems that the CPP of mNeonGreen starts to drop already at low $I_0$ and then continuously decreases throughout the laser powers scanned. A possible explanation could be that mNeonGreen is more susceptible to saturation mainly due to its relatively extinction coefficient of 116 000 M$^{-1}$ cm$^{-1}$. To confirm this assumption the fluorescence lifetime was the determined for mNeonGreen, EGFP and AcGFP.

## 5.2. Fluorescence Lifetime Measurements

The fluorescence lifetime of GFPs was determined using time-correlated single photon counting (TCSPC). Single fluorophores are excited by short laser pulses in the picosecond timerange and the time delay between the excitation pulse and the detection of the emitted photon is recorded. By repeating this procedure multiple times one obtains a distribution of the times the fluorophore spends in the excited state, which can then be fitted to an exponential decay function to extract the fluorescence lifetime of the specific fluorophore. The technique is complicated by the fact that the recorded correlation time between the pulse and the actual detection of the photon is a convo-

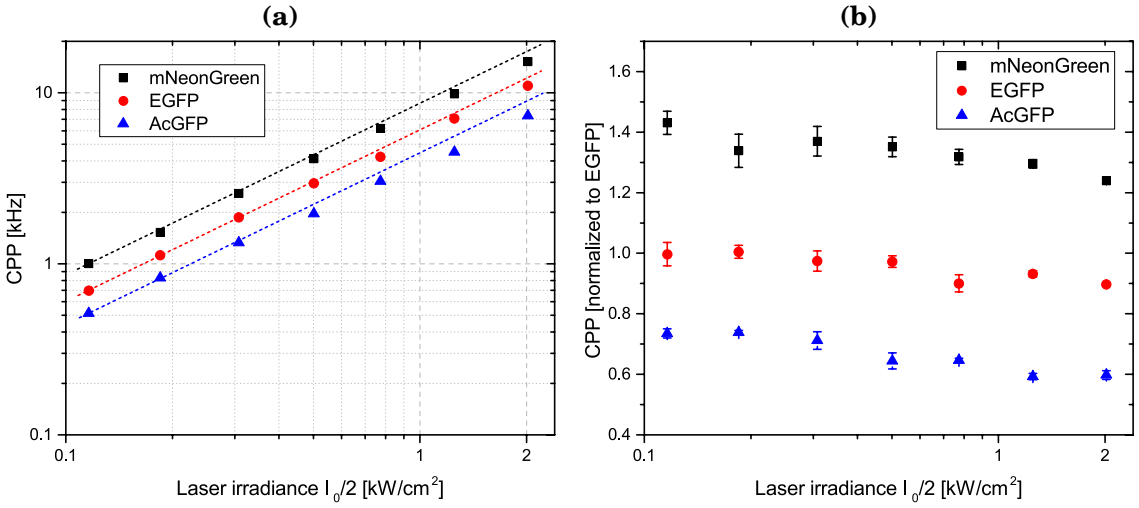


**Figure 5.3.: Molecular brightness for freely diffusing mNeonGreen, EGFP and AcGFP, as measured in FCS at different laser powers in an enlarged focus volume.**
In (a), data is fitted to a power law of type $ax^b$ (dashed lines), yielding values for $b$ close to 1 as expected for a single-photon excitation process. Normalization of the respective CPP values to the fit of EGFP illustrates the relative brightness of the fluorphores and the increasing deviation of data from the fit at high laser irradiances (b). Error bars indicate the standard deviation from 15 measurements with an acquisition time of 30 s.
The laser irradiance $I_0$ was estimated from the mean power of the laser beam $P$ and the beam waist $\omega_0 = 0.7\,\mu\text{m}$, determined by a reference measurement of ATTO488: $I_0 = 2P/(\pi\omega_0^2)$, $\lambda_{\text{exc}} = 488\,\text{nm}$, $T = 298\,\text{K}$.

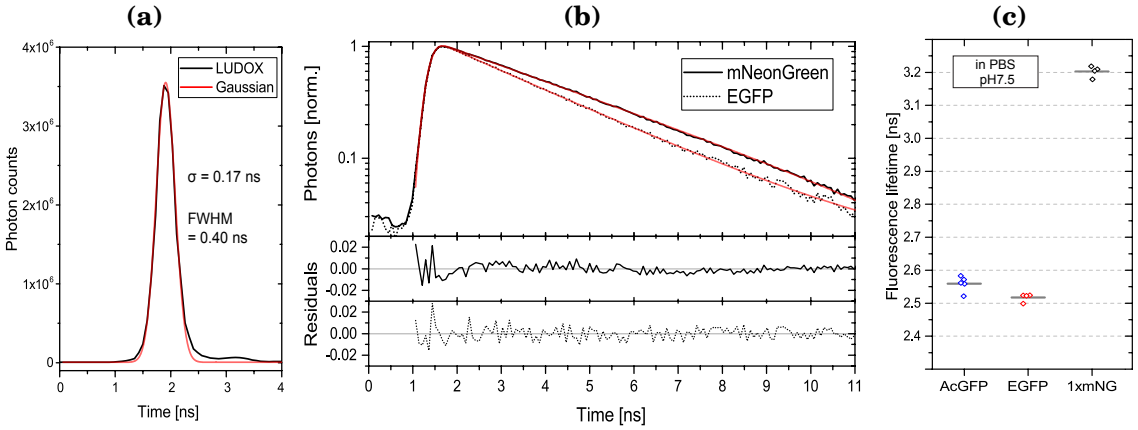


**Figure 5.4.: Fluorescence lifetime of GFP monomers measured with TCSPC-FLIM.** (a) Instrument response function (IRF) of the setup (b) the time trace of fluorescence emission is well described by a mono-exponential decay in PBS pH 7.5 for all constructs as can be seen from two exemplary curves in (b). Scatter plot on the right (c) shows that the fluorescence lifetime of mNeonGreen is increased by a factor of 25% with respect to EGFP and AcGFP under the conditions tested.

lution of both systematic time delays (finite laser pulse width, finite processing speed of the electronics) and the time delay of interest (fluorescence lifetime). This was accounted for by recording the instrument response function (IRF) with a scattering solution (LUDOX, Sigma-Aldrich). The IRF of the acquisition system is plotted in fig. 5.4a with a FWHM of 400 ps, which resembles the laser pulse duration. Approximating the IRF by a Gaussian allows the derivation of an analytical expression for the fitting function (see equation 2.24) by solving the convolution integal. The plateau of the IRF at longer correlation times is probably related to spontaneous emission of the laser (Leonard et al., 2014) and neglectable in amplitude. The width $\sigma = 170$ ps obtained from the IRF was kept fixed for all fits, which well described the measured fluorescence decays (see fig. 5.4b). In this way, deconvoluted values for the fluorescence lifetimes of each GFP variant were obtained (see fig. 5.4c).

While AcGFP and EGFP have similar fluorescence lifetimes of $(2.56 \pm 0.02)$ ns and $(2.52 \pm 0.01)$ ns, respectively, the lifetime of monomeric mNeonGreen is considerably higher with a value of $(3.20 \pm 0.02)$ ns.

This result confirms observations made in FCS that mNeonGreen is more viable to saturation not only due to a higher extinction coefficient, but also due to a 28 % longer residence time in the excited state compared to EGFP and AcGFP. This enhances the effect of ground state depletion and may make it relevant already at low excitation intensities.

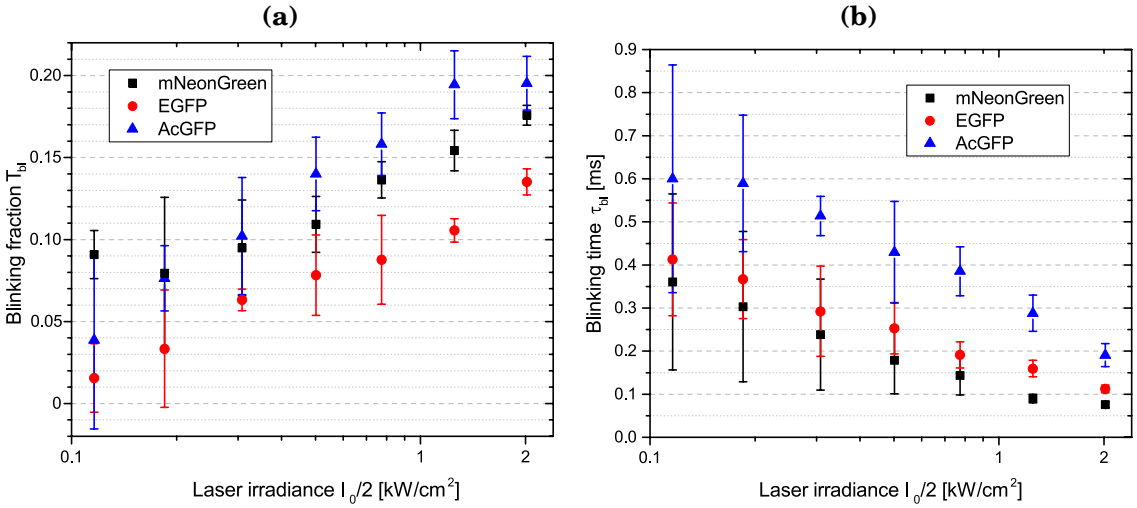


**Figure 5.5.: Power dependence of blinking fraction and blinking time for mNeonGreen, EGFP and AcGFP.**

## 5.3. Triplet and Blinking Dynamics of the GFP Variants

At laser powers exceeding 10 kW/cm$^2$ singlet-triplet transitions increase strikingly in amplitude and are the predominant photophysical contribution observable in the recorded correlation curves.

In the low irradiance regime, however, triplet fraction and triplet time do not show any trend for all three GFPs (see appendix A.2a and A.2b). The fraction of molecules, that occupy the triplet state is with 4% and 5% comparably small for mNeonGreen and AcGFP and practically not detectable, but significant for EGFP with on average 13 %.

Blinking is observable already at low excitation intensities and shows a similar behavior for all three GFP variants (see 5.5). The blinking times of mNeonGreen and EGFP are similar and range from 400 µs down to about 75 µs, whereas the time corresponding to AcGFP is in each case roughly 200 µs longer throughout the power range tested.

## 5.4. Protonation of the Chromophore

Besides the use of fluorophores as pH probes, the dynamical processes observed in FCS upon a change in pH can be used to gain information about the conformation and structure of the fluorophore.

To test the pH sensitivity of the three GFP variants, 10 mM potassium phosphate buffers with different pH values covering a range from 4 to 12 were prepared and sterile filtered. Outside the natural buffer capacity of phosphate buffer ranging from

pH 5.8 to pH 8, the pH value was adjusted by adding the required amounts of NaOH or HCl. GFP stock solutions were diluted to 15 nM in buffers of particular pH. The excitation intensity was set to 0.6 kW/cm$^2$.

Figure 5.6 shows the effect of two selected pH values on the shape of the measured correlation curves for all three GFP variants. At low pH, a dark state in the time range of the previously described blinking dominates the shape of the correlation functions for EGFP and AcGFP, with amplitudes of up to 400 %. Surprisingly, mNeonGreen response to pH is far less pronounced and, in addition, reversed. While the dark fraction increases with decreasing pH for EGFP and AcGFP, the opposite is observed for mNeonGreen. Moving from pH 11.0 to pH 4.5 reduces the fraction of molecules that are on average in a blinking state by 30 %. The diffusion time is independent on the pH of the buffer, with the exception that at highly acidic pH ($\leq 4.5$) the diffusion time decreases due to conformational changes of the protein structre or due to denaturation.

A more detailed analysis of the blinking fractions as a function of pH value is shown in figure 5.7a, which illustrates the striking differences of pH sensitivity between mNeonGreen and the other two GFP variants. At neutral to basic pH, the blinking fraction $T_{\mathrm{bl}}$ of EGFP and AcGFP remains constant with fractions of 9 % and 15 %, respectively. Below a pH value of about 7, the blinking fraction rises sharply for both GFPs reaching blinking fractions of over 80 % at pH 4. The dependence of the blinking fraction on pH is well described by a sigmoid function $F = A_0 + (A_1 - A_0)/(1 + 10^{\mathrm{p}K_{\mathrm{a}} - \mathrm{pH}})$; fitting $F$ to the data yields a p$K_{\mathrm{a}}$ of $5.3 \pm 0.1$ for AcGFP and a slightly higher p$K_{\mathrm{a}}$ of $5.7 \pm 0.1$ for EGFP. The latter result is in good agreement with a reported p$K_{\mathrm{a}}$ value of 5.8 based on fluorescence emission intensity measurements (Haupts et al., 1998).

As already mentioned before, mNeonGreen shows a completely different behavior when exposed to varying pH conditions. In contrast to EGFP and AcGFP, the magnitude of the blinking fraction $T_{\mathrm{bl}}$ is much less ranging from 5% to 25%. Additionally, the overall picture of the course of the blinking fraction is reversed: Opposite to the observations for EGFP and AcGFP, less molecules undergo blinking in acidic conditions, while at highly basic conditions the blinking fraction increases slightly above a broad plateau ranging from pH 5.5 to 10.0.

The behavior of the blinking fraction with changes in pH conditions directly affects the molecular brightness of each GFP variant, since molecules are not able to fluoresce as long as they are in a dark state. This is demonstrated by figure 5.7b, which shows the dependence of the counts per molecule (CPP) on pH. Comparing fig. 5.7a with 5.7b, one can tell that the progressivity of the CPP is a mirror image of the progressivity of the blinking fraction $T_{\mathrm{bl}}$. When the buffer becomes acidic, the CPP of

EGFP drops sharply from 5 kHz to roughly 2.2 kHz at pH 4.5. Likewise, the CPP of AcGFP drops from 3 kHz to below 0.8 kHz at low pH. The association of the blinking fraction and the molecular brightness is emphasized by also fitting the CPP data to the same sigmoid function $F$, which yield similar p$K_a$ values for all three constructs as were derived previously. The outlier at pH 4 for EGFP was excluded from the fitting process, as it is probably caused by denaturation (Kneen et al., 1998).

To exclude that the observed blinking dynamics are related to diffusional or photobleaching processes, correlation functions of mNeonGreen were recorded at an identical excitation density in a larger detection volume. This was achieved by increasing the underfilling factor from 5 to 6.7, leading to a beam waist shift of $\omega_0 = 0.7\,\text{nm}$ to $\omega_0 = 1.0\,\text{nm}$.

Figure 5.8 shows that the blinking fraction $T_{bl}$ as well as the blinking time $\tau_{bl}$ are independent of the focal volume size. This result confirms that the blinking dynamics seen in the correlation functions belong to inherent transient dark states of the fluorophore, which should correspondingly not depend on the geometry of the observation volume. Moreover, figure 5.9 shows the effect of different laser irradiances on the blinking fraction and the blinking time. It is demonstrated that blinking dynamics not only depend on the excitation power as discussed in the previous section, but also on the pH value of the buffer. The coupled dependency of the blinking dynamics of mNeonGreen on pH as well as illumination power differs from the behavior of EYFP, where the blinking time was not affected by excitation intensity (Schwille et al., 2000).

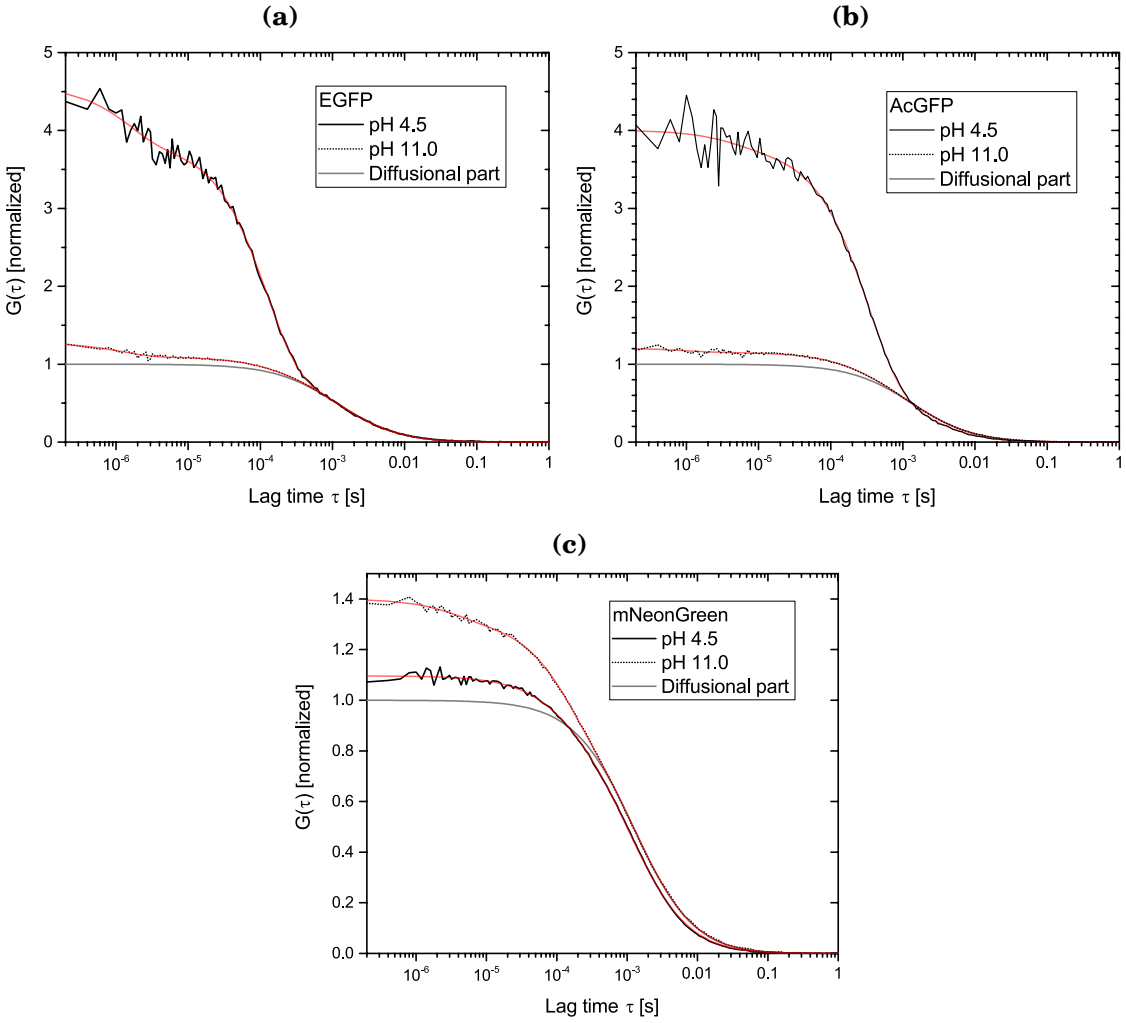


**Figure 5.6.: Exemplary correlation curves showing the effect of different pH on mNeonGreen, EGFP and AcGFP.**
From high to neutral pH, the correlation curves of EGFP (a) and AcGFP (b) are dominated by diffusion and are nearly unchanged, while at low pH ($\leq 7$) the fraction $T_{\mathrm{bl}}$ of molecules undergoing blinking grows strongly. In contrast, mNeonGreen's (c) response to a shift of the pH value from 11.0 to 4.5 is reversed and, additionally, far less pronounced. Measurements were performed at a laser irradiance of 0.6 kW/cm$^2$ in an observation volume with a beam waist of 0.7 µm. The correlation functions shown are the average of 30 – 60 repetitions with an acquisition time of 30 s.

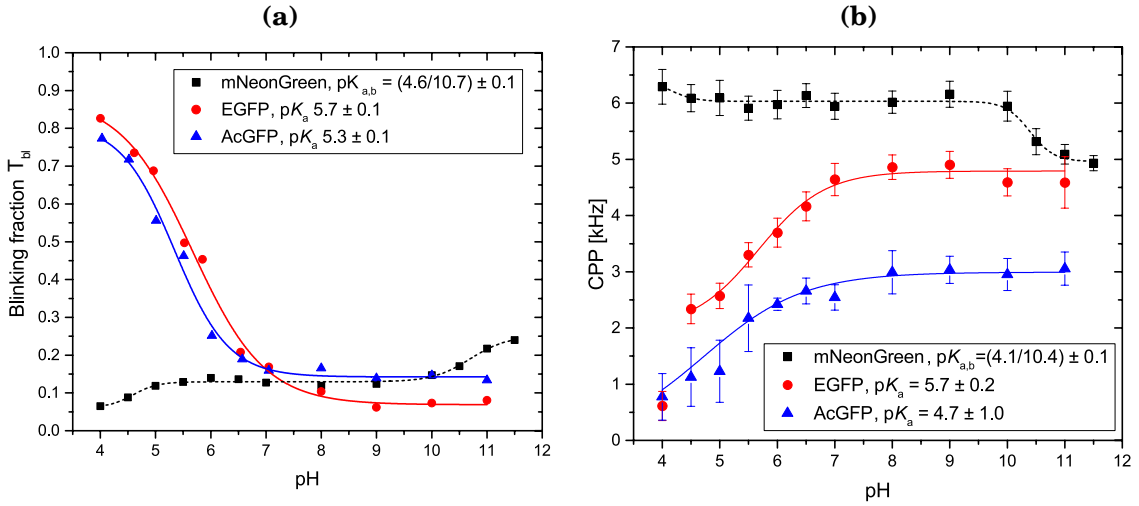


**Figure 5.7.: mNeonGreen's sensitivity to varying pH differs strongly from EGFP and AcGFP regarding blinking fraction and molecular brightness.**
(a) At low pH, a process in the time regime of blinking grows in amplitude similarly for EGFP and AcGFP by almost a factor of 4. This behavior of $T_{\mathrm{bl}}$ can be well described by sigmoidal dose-response functions, yielding a pKa of 5.7 for EGFP and 5.3 for AcGFP. Surprisingly, the fluorescence properties of mNeonGreen are far less affected by acidic or alkaline buffer conditions. Since higher fractions of molecules in a non-fluorescent state reduce the overall brightness, the behavior of CPP as a function of pH (b) is a mirror image of the progressivity of the blinking fraction $T_{\mathrm{bl}}$.

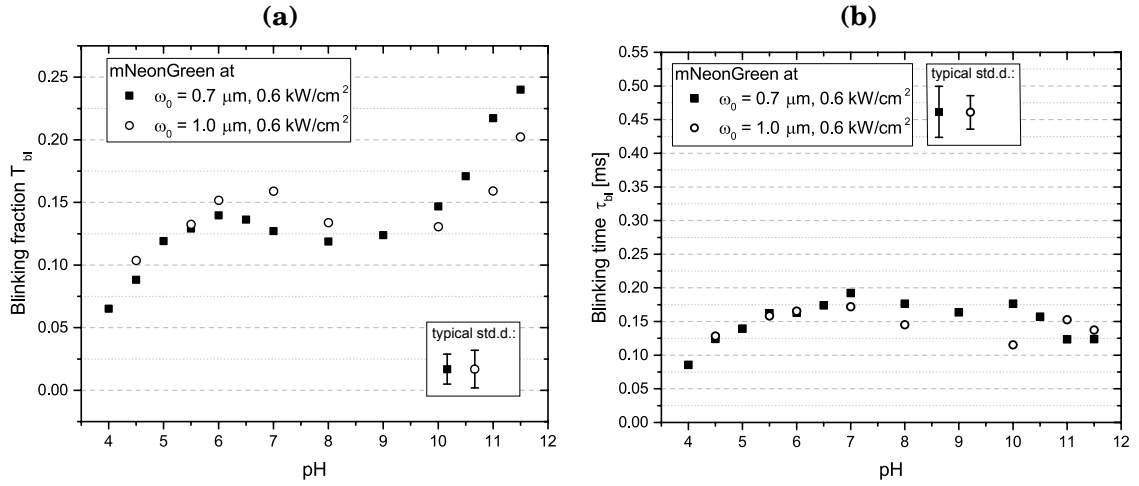


**Figure 5.8.: Blinking is not related to a diffusional process.**
Blinking fraction (a) and blinking time (b) were obtained from correlation curves recorded at two different focal volume sizes (0.7 µm and 1.0 µm) at identical excitation intensities. The blinking dynamics in mNeonGreen are unrelated to diffusion or photobleaching as the blinking time (b) is not affected by the size of the observation volume. Consistently, also the blinking fractions (a) under the two conditions tested match within the error margin.

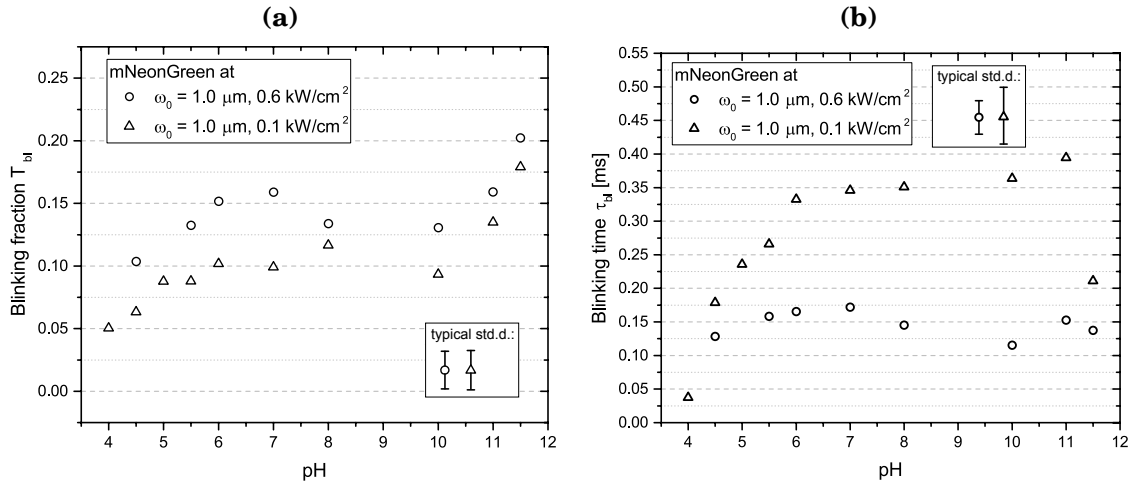


**Figure 5.9.: Interdependency of blinking fraction and blinking time on laser irradiance as well as pH.**
Blinking fraction (a) and blinking time (b) were obtained from correlation curves recorded at two different laser irradiances (0.1 kW/cm$^2$ and 0.6 kW/cm$^2$) in a detection volume with a beam waist $\omega_0 = 1.0\,\mu m$. The blinking fraction as well as the blinking time is dependent on the laser irradiance over the whole pH range similarly to the power series (see fig. 5.5) at pH 8, i.e. that the blinking fraction increases while the blinking time decreases with illumination power.

# 6. Fluorescence Spectroscopy of mNeonGreen Tandem Proteins

With this in mind, mNeonGreen tandems with up to five copies were successfully cloned and purified. To evaluate the suitability of multimerized mNeonGreen constructs for future single-molecule applications in TIRFM and FCS, the yield of fluorescence output which can be achieved is quantified. Additionally, the effect of oligomerization on the fluorescent lifetime and on the diffusion coefficient is determined in *in vitro* and *in vivo* assays.

## 6.1. Diffusional Properties of mNeonGreen Oligomers

### FCS Measurements in Aqueous Solution

Correlation functions of mNeonGreen oligomers diluted to 5 nM in 10 mM potassium phosphate buffer pH8 were recorded at power densities ranging from 0.1 – 2 kW/cm$^2$. The acquisition time was set to 60 s, and each measurement was repeated 15 times. The experiments were performed at room temperature at 23 °C, the temperature in the sample is assumed to be slightly warmer due to the applied laser irradiation ((25 ± 1) °C).

Figure 6.1 shows the correlation function of monomeric and pentameric mNeonGreen at the lowest and highest irradiance irradiance tested in this assay. The increased molecular size of the pentamer shifts the correlation function rightwards to longer times as the diffusion time through the observation volume increases. This is also observed for the correlation function measured at 2 kW/cm$^2$ but the increase in diffusion time appears to be less compared to the shift seen at 0.1 kW/cm$^2$. This suggests that the pentameric mNeonGreen is more affected by photobleaching than the monomeric mNeonGreen, either intrinsically or simply caused by the longer residence time in the detection volume and thus, longer exposure to the laser light.

The change in diffusion as the power increases was plotted in figure 6.2a. First of all it is evident that the diffusion time increases step-by-step with the multimerization state.Secondly, one can also identify a change in the progressivity of the diffusion times with increasing laser irradiances for the oligomers. While diffusion time of

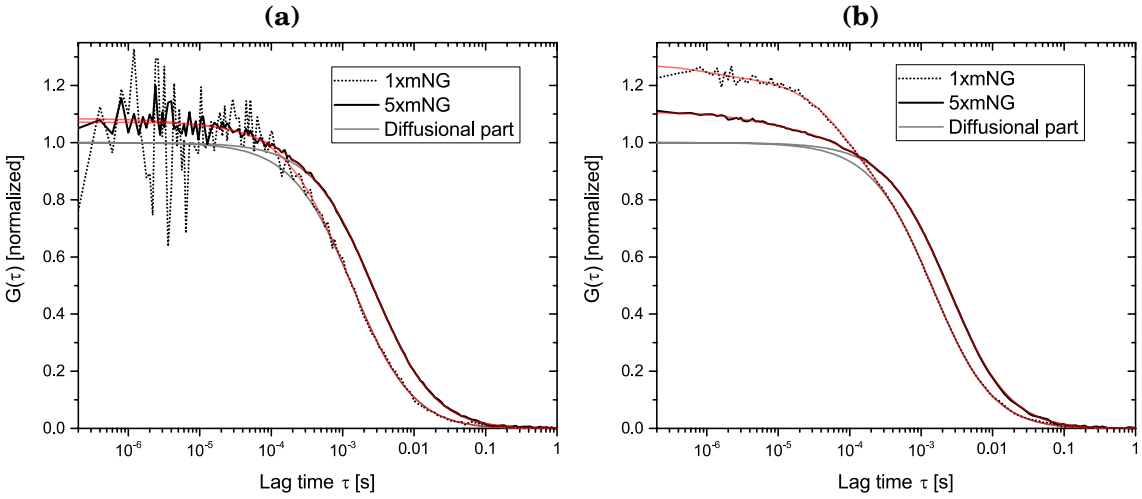


**Figure 6.1.: Exemplary correlation curves of monomeric and pentameric mNeonGreen.**
The effect of excitation intensity on the shape of the correlation function is shown for the lowest, 0.1 kW/cm$^2$ (a) and highest irradiance, 2.0 kW/cm$^2$ (b).

multimerized mNeonGreen gradually drops more for longer chains, the trend seen as the power increases for the monomer is inverted in terms of that is fairly constant or even slightly increasing. This suggests that while photobleaching is the dominant effect in mNeonGreen chains, monomeric mNeonGreen is mainly affected by saturation in the low irradiance regime.

To minimize photophysical influences in the derivation of diffusion coefficients, the diffusion time of each mNeonGreen oligomer was linearly extrapolated to zero light conditions (solid lines). The waist of the detection volume was determined to $\omega_0 = 0.72\,\mu m$ by a reference measurement of ATTO488 assuming a diffusion coefficient of 400 µm$^2$/s at 25 °C (Kapusta, 2010) and a fixed structural parameter of SP = 5. Figure 6.2b shows the calculated diffusion coefficients for mNeonGreen of varying chain lengths. Treating the mNeonGreen chain as perfect spheres, one expects a decrease of the diffusion coefficient proportional to $n^{-1/3}$, where $n$ stands for the number of subunits in the chain ($n = 1-5$). Despite the simple assumption made, the corresponding model fits the data surprisingly well (red line).

## FCS Measurements *in cellulo*

The diffusion coefficients of mNeonGreen oligomers were also quantified when expressed in living HEK293T cells growing on chambered glass slides.

The realization of FCS measurements in cells is impaired by the much more complex environment compared to *in vitro* assays, making it demanding for the experimentalist to record correlation functions of decent quality. A crucial requirement for suc-

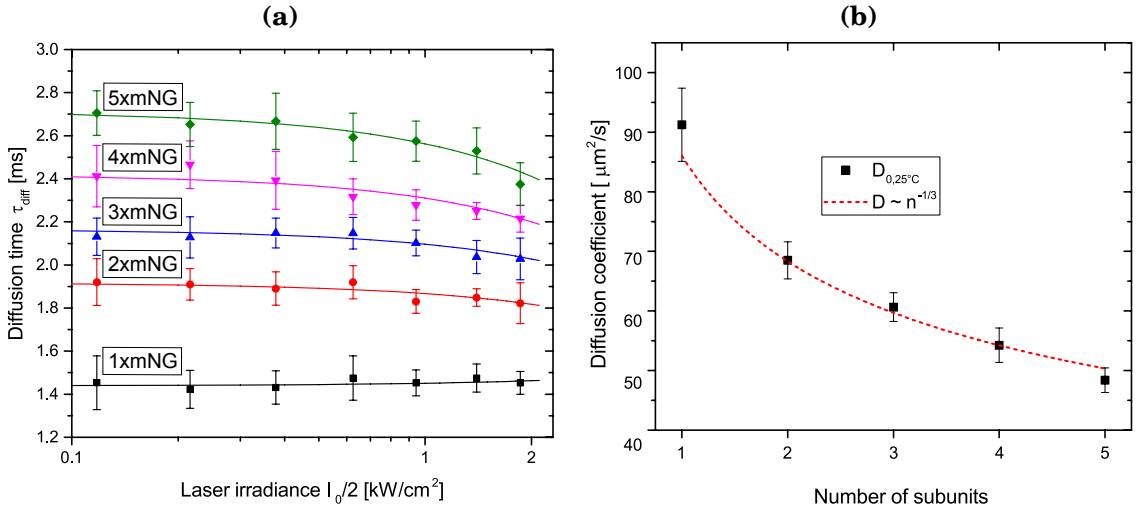


**Figure 6.2.: Diffusion coefficient of mNeonGreen oligomers in the low irradiance regime observed in FCS.**
(a) With increasing laser power, the diffusion time $\tau_{\text{diff}}$ of the multimerized mNeonGreen is dominated by photobleaching and decreases, whereas the diffusion time of the monomer stays constant or slightly rises due to saturation. The diffusion time of each oligomer was extrapolated to zero light conditions in order to obtain diffusion coefficients that are unaffected by photophysics (b). The dependence of the diffusion coefficient on the chain length $n$ is well described by a model assuming a spherical shape with a radius growing proportional to $n^{-1/3}$.

cessful intracellular FCS measurements is the positioning of the observation volume, both in the x-y-plane and in the z-direction (optical axis). Adjusting the focus position too high or too low will cause the the detection volume to stand out of the cellular compartment or to penetrate into the cover glass surface, which will in either case distort the shape of the detection volume and therefore affect the obtained diffusion time and fluorescence emission per molecule (CPP). Bearing in mind that in a confocal setup the length of the diffraction limited observation volume along the optical axis is about 1 µm and the height of a cell typically 4 µm – 10 µm, one has only a little margin for the focus position of at best 1 µm at central positions, but much less at peripheral regions.

Additional complication in intracellular FCS measurement is caused by the fact that the observed system is vivid and far from being in a steady-state or in an equilibrium as opposed to a aqueous buffer solution. Cellular compartments like vesicles or autofluorescent components in the cytoplasm may diffuse through the observation volume and cause additional fluctuating spikes in the fluorescence intensity time trace or lead to a slow decrease in overall signal due to continuous photobleaching of autofluorescent contaminants. This problem is accounted for by proficient placement among the cellular compartments and by reducing the measurement time in return of more repetitions.

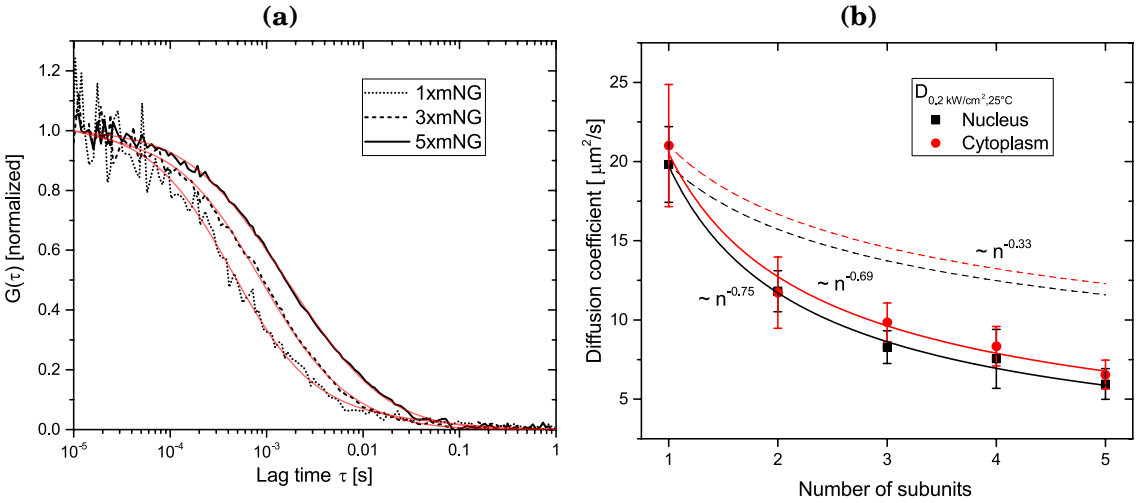


**Figure 6.3.: Diffusional properties of mNeonGreen oligomers in the nucleus and cytoplasm.**
The higher viscosity inside cells prolongs the diffusion time of monomeric mNeonGreen about 4-fold compared to an aqueous solution (compare with fig. 5.1a) as seen by the correlation curves (a) and by the diffusion coefficient (b). Moreover, larger particles undergo significantly more steric hindrance in cells, reducing the diffusion coefficient more drastically with chain length ($\propto n^{-0.7}$) compared to diffusion in phosphate buffer ($\propto n^{-0.33}$). Correlation curves were recorded with an acquisition time of 15 s and repeated 5 times for each cell ($n = 10$) and position (nucleus/cytoplasm). The beam waist was determined to equal 0.23 µm from a reference measurement of ATTO488 in water at 25 °C, which was used to estimate the laser irradiance according to fig. 5.2 as well as to calculate the respective diffusion coefficients. The applied laser irradiance was about 0.4 kW/cm$^2$, temperature and refractive index mismatches due to the cellular environment were neglected.

For this reason, a total of 10 cells with low to moderate expression levels were selected, recording five runs with an acquisition time of 15 s for each construct at room temperature (23 °C). Excitation intensity was adjusted so that monomeric mNeonGreen has a CPP of about 2 kHz in a diffraction limited detection volume, which lies in the low irradiance regime (≈0.4 kW/cm$^2$) to minimize photobleaching and photophysical artifacts to the fluorophores as well as to prevent photodamage to the cells.

Figure 6.3a shows representative correlation curves for monomeric, trimeric and pentameric mNeonGreen, all normalized to 1 at a lag time of 10 µs for better comparability. Due to the low excitation intensity used for the intracellular measurements, the contribution of singlet-triplet transitions was neglected and the correlation functions were fitted to a model describing the fluctuations due to diffusion and blinking only, whereby the latter was restricted to a time regime within 10 – 300 µs based on the results from the *in vitro* experiments.

As described in the previous section, the size of the observation volume was determined by measuring the diffusion time of ATTO488 in water, resulting in a beam

diameter of $\omega_0 = 0.23\,\mu m$. Neglecting potential temperature differences between the reference measurement at 25 °C and the measurements in cells, as well as corresponding refractive index mismatches due to the slightly increased refractive index in cells ($\approx 1.37$, Choi et al., 2007) compared to the immersion water (1.333), the corresponding diffusion coefficients of the mNeonGreen oligomers in the nucleus and in the cytoplasm are shown in fig. 6.3b. It is immediately noticeable that the progression of diffusion coefficients with chain lengths is significantly steeper compared to the situation in aqueous media, indicating a increased sterical hindrance especially for the larger molecules. The shift of diffusion coefficient of the monomeric mNeonGreen from $90\,\mu m^2/s$ down to $\approx 20\,\mu m^2/s$ serves as an indicator for the roughly 4.5 times higher viscosity in cells compared to an aqueous solution.

## 6.2. Effect of Oligomerization on Molecular Brightness

### FCS Measurements in Aqueous Solution

Analogously to section 5.1, the fluorescence emission per molecule (CPP) for each mNeonGreen oligomer was determined from the correlation data and plotted versus laser irradiance on a double-logarithmic scale (see fig. 6.4a). For a more direct quantitative comparison, fig. 6.4b shows the CPP normalized to the molecular brightness of a monomeric mNeonGreen as a function of illumination power.
The FCS analysis is complicated by the fact that each mNeonGreen molecule has a certain probability to be completely non-fluorescent due to deficient folding or maturation, which was determined by single-molecule bleaching step analysis to be 24%. If one assumes that this fraction, gained from the special case of a trimer, is a property of the (monomeric) mNeonGreen itself and not affected by the process of oligomerization, the examined solution of multimers is a mixture of multimers with binomially distributed numbers of fluorescent and non-fluorescent subunits. This affects not only the fluorescence signal, but also the amplitude of the correlation function and therefore the derived quantities like molecular brightness (see calculations in section 2.2.3 for details).

### FCS Measurements *in cellulo*

As a primary observation it can be stated from looking at exemplary fluorescence microscope images (fig. 6.5a) that the mNeonGreen monomer shows a homogeneous distribution among the cells comparable to that of EGFP and AcGFP when expressed in the cytoplasm without any visible aggregation or clustering artifacts.
To address the performance regarding molecular brightness of the monomeric GFP

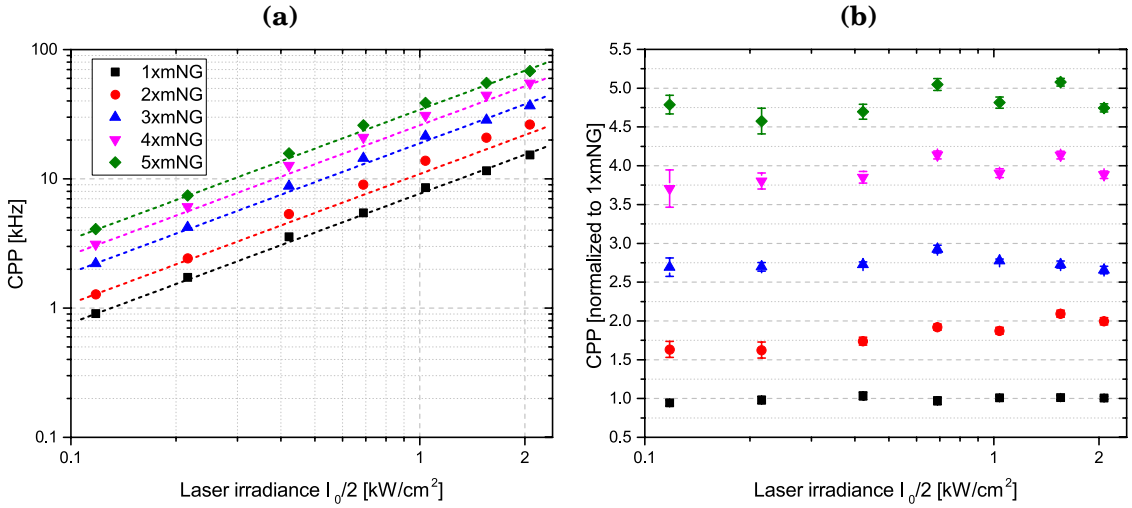


**Figure 6.4.: Derived molecular brightness (CPP′) of freely diffusing mNeonGreen oligomers measured at different laser irradiances in an enlarged observation volume (a).**
Assuming an inherent probability $p = 76\%$ that a random mNeonGreen monomer lacks fluorescent ability as seen in single-molecule TIRF, each chain itself consists of a mixture of molecules with binomially distributed numbers of fluorescent and non-fluorescent subunits. This complication was accounted for by weighting the amplitude of the diffusional part of the correlation function $G_D(0)$ based on the brightness of each species according to eq. 2.17.
The first three data points are fitted to a power law of type $ax^b$ (dashed lines). Normalization of the CPP′ data to the fit of the monomeric CPP illustrates the proportional increase of brightness according to chain lengths, independent of the excitation intensities tested (b). Values are mean ± std.d.

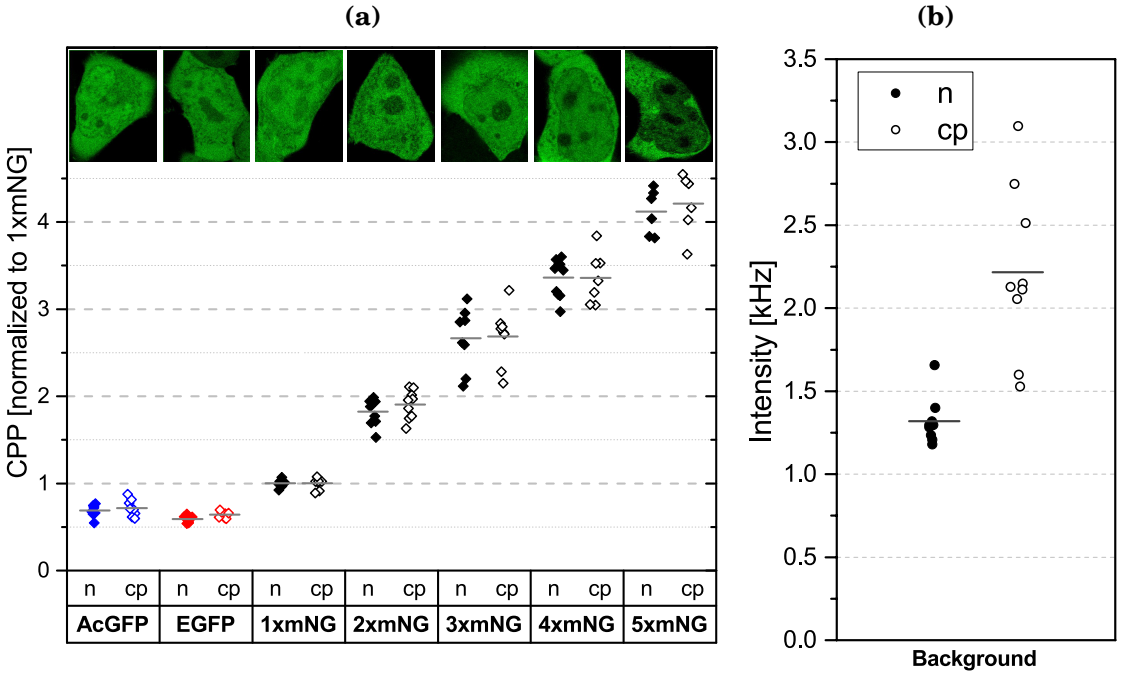


**Figure 6.5.: Molecular brightness of AcGFP, EGFP and mNeonGreen oligomers obtained in intracellular FCS measurements.**
The absolute value of 1xmNeonGreen, to which the plot is normalized to, is 2.58 kHz. Each dot corresponds to the mean CPP calculated for a single cell, obtained from 2 – 5 correlation curves recorded with a duration of 15 s depending on data quality. In the fitting routine, singlet-triplet transitions were neglected and blinking contributions were restricted to a time range between 10 µs and 250 µs according to *in vitro* experiments. Noticeable scatter of CPP-values reflects the complication of FCS analysis by the complex cellular environment in addition to cell-to-cell differences in background contributions (b) caused by cellular autofluorescence.

variants and the mNeonGreen chain inside cells, FCS measurements positioned in the nucleus and in the cytoplasm were performed. For each variant, a total of 10 cells with low to moderate expression levels were selected, recording five runs with an acquisition time of 15 s each. Excitation intensity was adjusted so that monomeric mNeonGreen has a fluorescence of about 2 kHz per molecule, which lies in the low irradiance regime (≈0.2 kW/cm$^2$) to prevent photobleaching of the fluorophores as well as photodamage to the cells.

## 6.3. Effect of Oligomerization on Fluorescence Lifetime

Fluorescence lifetime measurements were repeated analogously to section 5.2 to test the influence of cellular environment and of multimerization on the fluorescence lifetime on the GFP constructs.

As figure 6.6 shows, the fluorescence lifetime decreased for all constructs when moved form PBS to cells. The differences in fluorescence lifetime due to the different environmental conditions seems to be more pronounced for mNeonGreen compared to EGFP and AcGFP. Therefore, the ratio of fluorescence lifetime measured in PBS to the lifetime measured in cells was calculated and plotted in figure 6.7a, which illustrates the above-mentioned observation. Further, the fluorescence lifetime of the mNeonGreen seems to be reduced by a constant factor of 0.93 for both the *in vitro* and the *in vivo* measurements with increasing chain length. This finding reflects the fact that the increase of FRET efficiency $E = 1 - \tau_{da}/\tau_{d}$ occurring with an increase in mNeonGreen chain length is independent of the two conditions tested (see fig. 6.7b) and probably caused by multimerization only. The overall decrease in fluorescence lifetime is low and thus, the FRET efficiency reaches only up to 8%. This can be explained by the high quantum yield reported for mNeonGreen (N. C. Shaner et al., 2013), which makes non-radiative de-excitation pathways improbable.

## 6.4. Blinking Dynamics in Multimerized mNeonGreen

Besides the increase in diffusion time in the correlation curves shown in fig. 6.1 due to the increased chain length, one can further observe a difference in the blinking behavior between the monomer and the pentamer at $2\,\mathrm{kW/cm^2}$. At low excitation intensity there is practically no contribution from a dark state present in both mNeonGreen constructs displayed. At high laser irradiance one can see that oligomerization seems to reduce the fraction of molecules undergoing blinking. To look into the dependence of the blinking process on the state of multimerization, the fraction of molecules undergoing blinking was plotted for 1x – 5x mNeonGreen as a function of excitation intensity (see fig. 6.8a). While $T_{bl}$ increases monotonously for the monomeric mNeonGreen as already seen in section 5.3, the progressivity is far less pronounced for the dimeric mNeonGreen and completely independent (3x mNeonGreen) on illumination power or even reversed in a sense that the blinking fraction decreases with laser power (4x/5x mNeonGreen).
The blinking time $\tau_{bl}$ decreases for all oligomers with excitation intensity, and seems to be systematically shorter the more subunits are present in a chain (see fig. 6.8b).

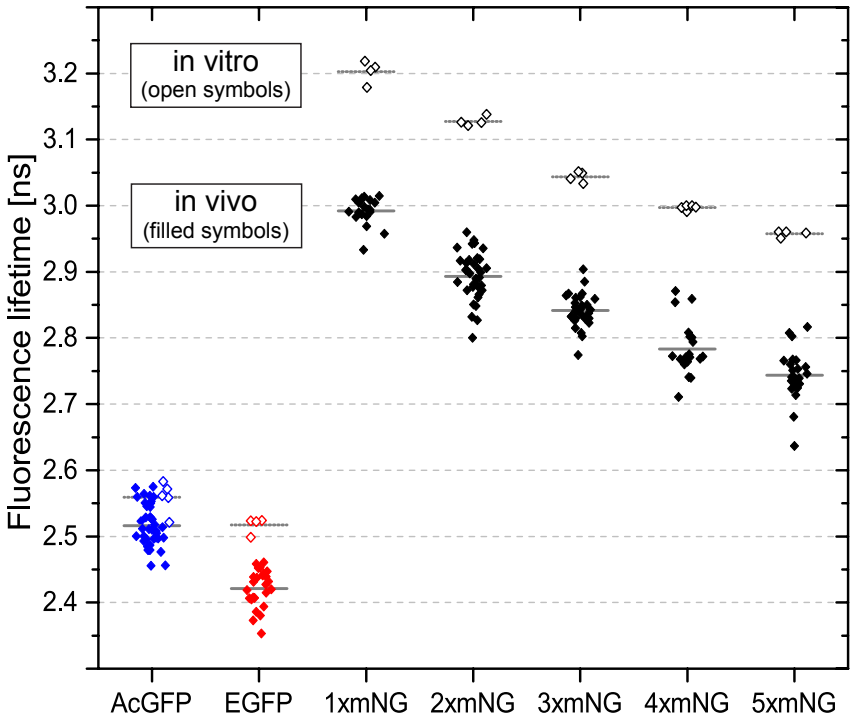


**Figure 6.6.: Fluorescence lifetime of GFP monomers and mNeonGreen chain as measured with TCSPC *in vitro* and *in vivo*.**
Scatter plot showing the lifetimes in PBS ($n$ = 4 – 5) and in HEK293T cells ($n$ = 20 – 39) obtained from fitting. The time trace of fluorescence emission is well described by a mono-exponential decay both in PBS pH7.5 and in cells for all constructs as can be seen from three exemplary curves in (a). Scatter plot showing the fluorescence lifetimes in PBS ($n$ = 4 – 5) and in HEK293T cells ($n$ = 20 – 39) obtained by TCSPC. While AcGFP and EGFP have similar fluorescence lifetimes with a minor discrepancy between the two conditions tested, the lifetime of mNeonGreen is about 25 % longer with a significant drop when moving from PBS to cells.

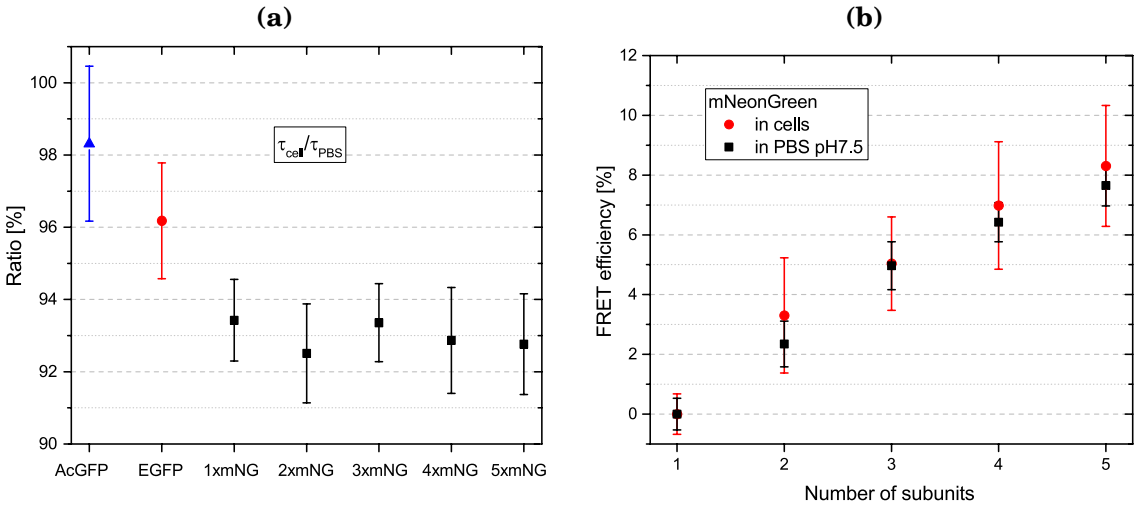


**Figure 6.7.: Homo-FRET occurring in mNeonGreen tandems increases with chain length**.
The proportionality of quantum yield to fluorescence lifetime indicates a reduced fluorescence emission per molecule by approximately 7 % for mNeonGreen, independent on the chain length, 4 % for EGFP and 2 % for AcGFP (a). The shortening of fluorescence lifetime by multimerization is used to estimate the fraction of FRET occurring in each oligomer, reaching up to 8 % in the mNeonGreen pentamer.

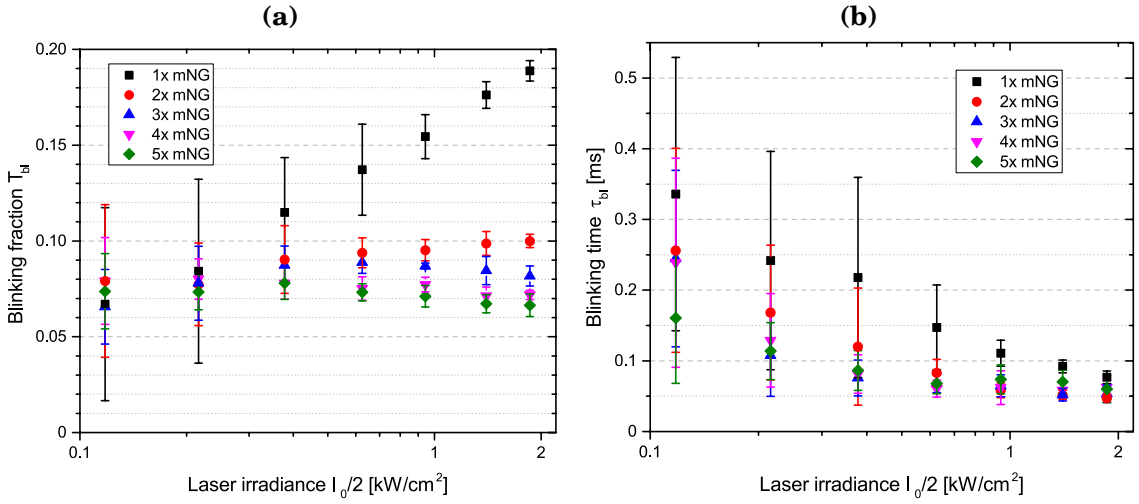


**Figure 6.8.: Dependence of blinking amplitude and blinking time on excitation intensity for mNeonGreen multimers (1x – 5x).**
For the mNeonGreen monomer the blinking fraction $T_{bl}$ (a) increases linearly with laser power in a logarithmic plot as seen in fig. 5.5a, whereas in a multimerized protein chain the amplitude seems to be independent or only weakly dependent on excitation intensity. Even though the data is subject to variation at low excitation, relaxation from the blinking state $\tau_{bl}$ (b) seems to be accelerated in the multimerized constructs. At higher excitation intensities, the respective blinking times converge progressively and coincide at about 60 µs. Values are mean ± std.d. of 15 measurements with an acquisition time of 30 s.

# 7. Conclusion

In this study, purified fluorescent proteins EGFP, AcGFP, mNeonGreen, and multimerized tandems of mNeonGreen were characterized with single-molecule techniques. Applying FCS in free solution, variation of pH as well as excitation power revealed significant differences between mNeonGreen and the two other GFP variants, thus reflecting the phylogenetic distances between the source organisms. The molecular brightness of mNeonGreen is increased 1.4-fold with respect to EGFP and 2.0-fold with respect to AcGFP under the same 488 nm excitation. This ratio was maintained over the whole range of typical excitation intensities (0.1-2 kW/cm2). The 1.4-fold increase is slightly less than what one would expect based on extinction coefficient and quantum yield (1.63) reported for mNeonGreen (N. C. Shaner et al., 2013). This discrepancy might be explained by the onset of saturation effects even at moderate laser powers due to the exceptionally high extinction coefficient. Consistent with mNeonGreen to be prone to ground state depletion, the fluorescence lifetime of mNeonGreen (3.2 ns) is slightly longer than for EGFP (2.5 ns). Alternatively, a reduced molecular brightness may be a result of photobleaching. Single-molecule TIRF microscopy showed that mNeonGreen decays three times faster than EGFP or AcGFP, although improved photostability was claimed based on wide-field microscopy (N. C. Shaner et al., 2013). A statistical analysis of bleach-steps in single-molecule imaging with trimeric mNeonGreen constructs allowed to estimate that 76% of the mNeonGreen domains were fully matured and fluorescent after purification.

As it is known for long, both AcGFP and EGFP show characteristic quenching in acidic buffers due to highly populated dark states, of up to 90% in pH 4.0 (Haupts et al., 1998; Widengren, Terry and Rigler, 1999). Surprisingly, mNeonGreen showed a much different behaviour. The magnitude of blinking fractions leading to a quenched total fluorescence never exceeds 25%. In stark contrast, the progression of pH-dependence is reversed: a negligible fraction of molecules occupy dark states under acidic conditions, blinking amplitudes are constant between a pH value of 5 and 10, and finally rise in the basic regime. This behaviour is inconsistent with the canonical view of external protonation dependent conformational changes. It seems protons cannot enter the mNeonGreen barrel to protonate the phenolic hydroxy group of the central Tyrosin in the chromophore (Haupts et al., 1998). Once a crystal structure will

be available, it would be interesting to clarify, whether the topology of the hydrogen bonding network excludes transfer of protons from the surface into the interior of the protein. Finally, spectroscopic studies on point mutants targeting the chromophore environment may uncover why the pH-depen-dence of mNeonGreen is so much different than that of EYFP, although both proteins share the same amino acid sequence undergoing cyclization (GYG) (Schwille et al., 2000).

One obvious strategy to improve the signal-to-noise in single-molecule applications is the use of multimeric fluorescent proteins as fluorescent labels. Here, we studied constructs with up to five mNeonGreen domains connected by a short linker. The normalized molecular brightness as reflected by CPP-values in FCS indeed showed a linear rise with a slope of almost one. Recently, a similar brightness standard was introduced based on a tetrameric EGFP chain, albeit with a smaller brightness increment (Vamosi et al., 2016). This means, with mNeonGreen, each additional FP domain in the tandem construct increased the signal by a quantum corresponding the fluorescence yield of the monomer. Typical limitations as inner filter effects or reduced quantum yield due to homotypic FRET seem to be negligible. This property was reproduced even inside cells, in the cytoplasm and the nucleus, where larger viscosity aggravates photobleaching especially of larger protein constructs. Because the molecular brightness scales linearly with the number of mNeonGreen domains in the protein such chains could be used as a reference to address the stoichiometry of complex binding reactions.

# A. Appendix

## A.1. TIRFM

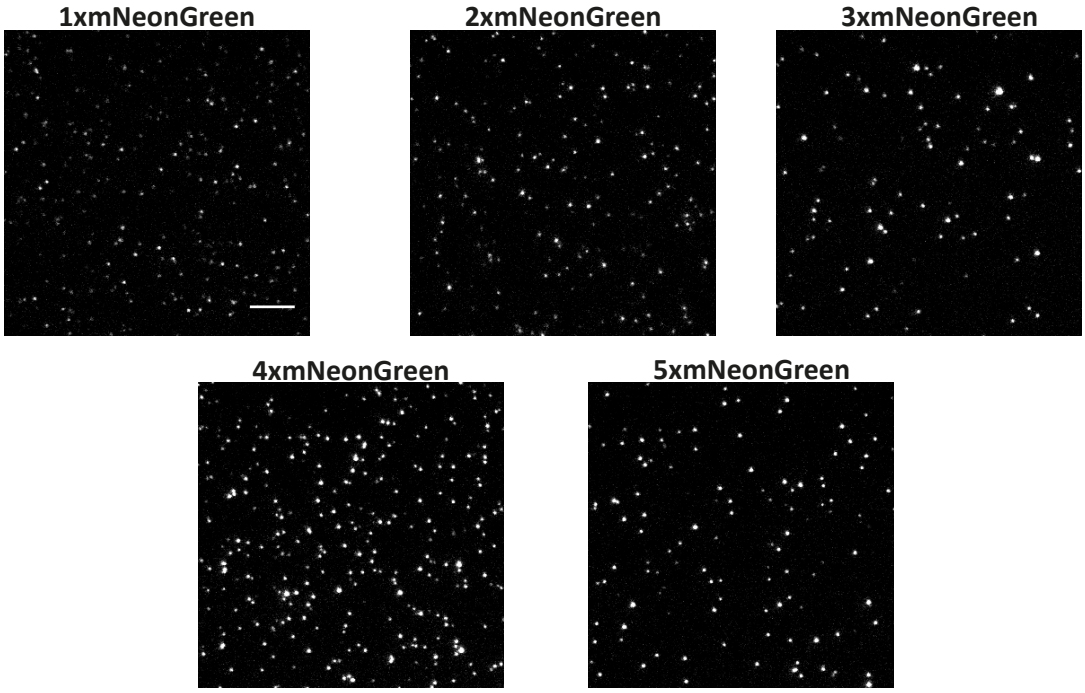


**Figure A.1.: TIRF images of mNeonGreen oligomers.**

## A.2. FCS

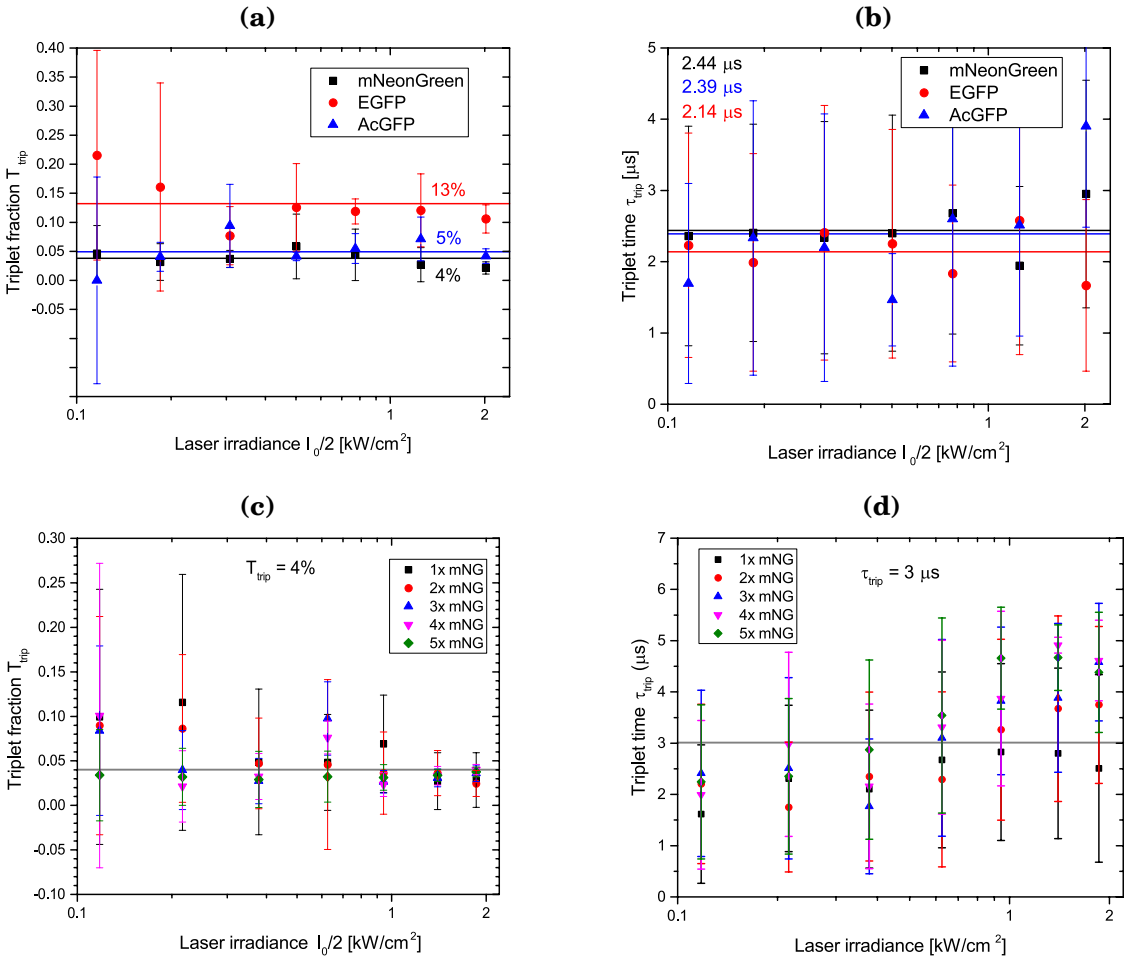


**Figure A.2.: Triplet fraction and time of monomeric GFPs and the mNeonGreen chain**

# Bibliography


Austen, Katharina et al. (2015). 'Extracellular rigidity sensing by talin isoform-specific mechanical linkages'. In: *Nat Cell Biol* 17.12, pp. 1597–1606. ISSN: 1465-7392. DOI: 10.1038/ncb3268http://www.nature.com/ncb/journal/v17/n12/abs/ncb3268.html#supplementary-information. URL: http://dx.doi.org/10.1038/ncb3268.

Chattoraj, M. et al. (1996). 'Ultra-fast excited state dynamics in green fluorescent protein: multiple states and proton transfer'. In: *Proc Natl Acad Sci U S A* 93.16, pp. 8362–7. ISSN: 0027-8424 (Print) 0027-8424 (Linking). URL: http://www.ncbi.nlm.nih.gov/pubmed/8710876.

Choi, Wonshik et al. (2007). 'Tomographic phase microscopy'. In: *Nat Meth* 4.9, pp. 717–719. ISSN: 1548-7091. DOI: http://www.nature.com/nmeth/journal/v4/n9/suppinfo/nmeth1078_S1.html. URL: http://dx.doi.org/10.1038/nmeth1078.

Cody, C. W. et al. (1993). 'Chemical-Structure of the Hexapeptide Chromophore of the Aequorea Green-Fluorescent Protein'. In: *Biochemistry* 32.5, pp. 1212–1218. ISSN: 0006-2960. DOI: Doi10.1021/Bi00056a003. URL: %3CGo%20to%20ISI%3E://WOS:A1993KL45800003%20http://pubs.acs.org/doi/pdfplus/10.1021/bi00056a003.

Cubitt, A. B. et al. (1995). 'Understanding, improving and using green fluorescent proteins'. In: *Trends Biochem Sci* 20.11, pp. 448–55. URL: http://www.ncbi.nlm.nih.gov/entrez/query.fcgi?cmd=Retrieve&db=PubMed&dopt=Citation&list_uids=8578587.

Dopf, Jill and Thomas M. Horiagon (1996). 'Deletion mapping of the Aequorea victoria green fluorescent protein'. In: *Gene* 173.1. Flourescent Proteins and Applications, pp. 39–44. ISSN: 0378-1119. DOI: http://dx.doi.org/10.1016/0378-1119(95)00692-3. URL: http://www.sciencedirect.com/science/article/pii/0378111995006923.

Dross, N. et al. (2009). 'Mapping eGFP oligomer mobility in living cell nuclei'. In: *PLoS One* 4.4, e5041. ISSN: 1932-6203 (Electronic) 1932-6203 (Linking). DOI: 10.1371/journal.pone.0005041. URL: http://www.ncbi.nlm.nih.gov/pubmed/19347038.

Gingell, D., O.S. Heavens and J.S. Mellor (1987). 'General electromagnetic theory of total internal reflection fluorescence: the quantitative basis for mapping cell-substratum topography'. In: *Journal of Cell Science* 87.5, pp. 677–693. ISSN: 0021-9533. eprint: http://jcs.biologists.org/content/87/5/677.full.pdf. URL: http://jcs.biologists.org/content/87/5/677.

Haupts, U. et al. (1998). 'Dynamics of fluorescence fluctuations in green fluorescent protein observed by fluorescence correlation spectroscopy'. In: *Proc Natl Acad Sci U S A* 95.23, pp. 13573–8. ISSN: 0027-8424 (Print). URL: http://www.ncbi.nlm.nih.gov/entrez/query.fcgi?cmd=Retrieve&db=PubMed&dopt=Citation&list_uids=9811841.

Kapusta, Peter (2010). *Absolute Diffusion Coefficients: Compilation of Reference Data for FCS Calibration*. [Online; accessed 27-March-2016]. URL: http://www.picoquant.com/images/uploads/page/files/7353/appnote_diffusioncoefficients.pdf.

Kneen, Malea et al. (1998). 'Green Fluorescent Protein as a Noninvasive Intracellular pH Indicator'. In: *Biophysical Journal* 74.3, pp. 1591–1599. ISSN: 0006-3495. DOI: http://dx.doi.org/10.1016/S0006-3495(98)77870-1. URL: http://www.sciencedirect.com/science/article/pii/S0006349598778701.

Leonard, Jeremie et al. (2014). 'High-throughput time-correlated single photon counting'. In: *Lab Chip* 14 (22), pp. 4338–4343. DOI: 10.1039/C4LC00780H. URL: http://dx.doi.org/10.1039/C4LC00780H.

Müller, Paul, Schwille and Thomas Weidemann (2014). 'PyCorrFit—generic data evaluation for fluorescence correlation spectroscopy'. In: *Bioinformatics* 30.17, pp. 2532–2533. DOI: 10.1093/bioinformatics/btu328. eprint: http://bioinformatics.oxfordjournals.org/content/30/17/2532.full.pdf+html. URL: http://bioinformatics.oxfordjournals.org/content/30/17/2532.abstract.

Ormo, M. et al. (1996). 'Crystal structure of the Aequorea victoria green fluorescent protein'. In: *Science* 273.5280, pp. 1392–5. ISSN: 0036-8075 (Print). URL: http://www.sciencemag.org/cgi/content/abstract/273/5280/1392%20http://www.ncbi.nlm.nih.gov/entrez/query.fcgi?cmd=Retrieve&db=PubMed&dopt=Citation&list_uids=8703075.

Pack, C. et al. (2006). 'Microenvironment and effect of energy depletion in the nucleus analyzed by mobility of multiple oligomeric EGFPs'. In: *Biophysical Journal* 91.10, pp. 3921–3936. ISSN: 0006-3495. DOI: 10.1529/biophysj.105.079467. URL: %3CGo%20to%20ISI%3E://WOS:000241702500037.

Petrov, E. P. and Schwille (2008). 'State of the Art and Novel Trends in Fluorescence Correlation Spectroscopy'. In: *Standardization and Quality Assurance in Fluorescence Measurements II: Bioanalytical and Biomedical Applications*. Ed. by Ute

Resch-Genger. Berlin, Heidelberg: Springer Berlin Heidelberg, pp. 145–197. ISBN: 978-3-540-70571-0. DOI: 10.1007/4243_2008_032. URL: http://dx.doi.org/10.1007/4243_2008_032.

Schwille et al. (2000). 'Fluorescence correlation spectroscopy reveals fast optical excitation-driven intramolecular dynamics of yellow fluorescent proteins'. In: *Proc Natl Acad Sci U S A* 97.1, pp. 151–6. ISSN: 0027-8424 (Print). URL: http://www.ncbi.nlm.nih.gov/entrez/query.fcgi?cmd=Retrieve&db=PubMed&dopt=Citation&list_uids=10618386.

Shaner, N. C. et al. (2013). 'A bright monomeric green fluorescent protein derived from Branchiostoma lanceolatum'. In: *Nat Methods* 10.5, pp. 407–9. ISSN: 1548-7105 (Electronic) 1548-7091 (Linking). DOI: 10.1038/nmeth.2413. URL: http://www.ncbi.nlm.nih.gov/pubmed/23524392.

Shaner, Nathan C., Robert E. Campbell et al. (2004). 'Improved monomeric red, orange and yellow fluorescent proteins derived from Discosoma sp. red fluorescent protein'. In: *Nat Biotech* 22.12, pp. 1567–1572. ISSN: 1087-0156. DOI: http://www.nature.com/nbt/journal/v22/n12/suppinfo/nbt1037_S1.html. URL: http://dx.doi.org/10.1038/nbt1037.

Shaner, Nathan C., Michael Z. Lin et al. (2008). 'Improving the photostability of bright monomeric orange and red fluorescent proteins'. In: *Nat Meth* 5.6, pp. 545–551. ISSN: 1548-7091. DOI: http://www.nature.com/nmeth/journal/v5/n6/suppinfo/nmeth.1209_S1.html. URL: http://dx.doi.org/10.1038/nmeth.1209.

Ulbrich, M. H. and E. Y. Isacoff (2007). 'Subunit counting in membrane-bound proteins'. In: *Nat Methods* 4.4, pp. 319–21. ISSN: 1548-7091 (Print) 1548-7091 (Linking). DOI: 10.1038/nmeth1024. URL: http://www.ncbi.nlm.nih.gov/pubmed/17369835%20http://www.nature.com/nmeth/journal/v4/n4/pdf/nmeth1024.pdf.

Valeur, Bernard (2001). 'Introduction'. In: *Molecular Fluorescence*. Wiley-VCH Verlag GmbH, pp. 3–19. ISBN: 9783527600243. DOI: 10.1002/3527600248.ch1. URL: http://dx.doi.org/10.1002/3527600248.ch1.

Vamosi, G. et al. (2016). 'EGFP oligomers as natural fluorescence and hydrodynamic standards'. In: *Sci Rep* 6, p. 33022. ISSN: 2045-2322 (Electronic) 2045-2322 (Linking). DOI: 10.1038/srep33022. URL: http://www.ncbi.nlm.nih.gov/pubmed/27622431.

Visser, Antonie J.W.G. and Olaf J. Rolinski (2014). *Basic Photophysics*. [Online; accessed 7-November-2016]. URL: %5Curl%7Bhttp://photobiology.info/Visser-Rolinski.html%7D.

Ward, William W. and Stephen H. Bokman (1982). 'Reversible denaturation of Aequorea green-fluorescent protein: physical separation and characterization of the renatured protein'. In: *Biochemistry* 21.19, pp. 4535–4540. ISSN: 0006-2960. DOI: 10.1021/bi00262a003. URL: http://dx.doi.org/10.1021/bi00262a003.

Weidemann, Thomas, Jonas Mücksch and Schwille (2014). 'Fluorescence fluctuation microscopy: a diversified arsenal of methods to investigate molecular dynamics inside cells'. In: *Current Opinion in Structural Biology* 28, pp. 69–76. ISSN: 0959-440X. DOI: http://dx.doi.org/10.1016/j.sbi.2014.07.008. URL: http://www.sciencedirect.com/science/article/pii/S0959440X14000803.

Weidemann, Thomas, Malte Wachsmuth et al. (2003). 'Counting Nucleosomes in Living Cells with a Combination of Fluorescence Correlation Spectroscopy and Confocal Imaging'. In: *Journal of Molecular Biology* 334.2, pp. 229–240. ISSN: 0022-2836. DOI: http://dx.doi.org/10.1016/j.jmb.2003.08.063. URL: http://www.sciencedirect.com/science/article/pii/S0022283603010775.

Widengren, J., U. Mets and R. Rigler (1999). 'Photodynamic properties of green fluorescent proteins investigated by fluorescence correlation spectroscopy'. In: *Chemical Physics* 250.2, pp. 171–186. ISSN: 0301-0104. DOI: Doi10.1016/S0301-0104(99)00255-4. URL: %3CGo%20to%20ISI%3E://WOS:000084531100006%20http://ac.els-cdn.com/S0301010499002554/1-s2.0-S0301010499002554-main.pdf?_tid=ec04bbac-6919-11e6-8130-00000aab0f01&acdnat=1471947253_ab8c4935f4ce4e4efb9b0e4cee30b8d0.

Widengren, J., B. Terry and R. Rigler (1999). 'Protonation kinetics of GFP and FITC investigated by FCS - aspects of the use of fluorescent indicators for measuring pH'. In: *Chemical Physics* 249.2-3, pp. 259–271. ISSN: 0301-0104. URL: %3CGo%20to%20ISI%3E://000084102700015.

Yang, Fan, Larry G. Moss and George N. Phillips (1996). 'The molecular structure of green fluorescent protein'. In: *Nat Biotech* 14.10, pp. 1246–1251. URL: http://dx.doi.org/10.1038/nbt1096-1246.

# Acknowledgements

First, I thank Prof. Dr. Petra Schwille for giving me the opportunity to work in her research group.

I would also like to acknowledge Prof. Dr. Matthias Rief for accepting to be my supervisor at TUM.

I am deeply grateful to Dr. Thomas Weidemann for all his efforts throughout the last year. Personally, I can not think of a better advisor and supervisor for my thesis.

I also want to thank Dr. Eugene Petrov for his critical input, Dr. Armin Lambacher for sharing his knowledge regarding single-molecule TIRF, Sandra Lemke for her assistance in the FLIM experiments and, last but not least, Magnus-Carsten Huppertz for his efforts in purifying the GFPs.

Moreover, I want to thank the whole group for creating an enjoyable atmosphere, and especially Dr. Henri Franquelim for his overall helpfulness.

# Selbstständigkeitserklärung

Hiermit erkläre ich, dass ich die vorliegende Arbeit selbstständig angefertigt, nicht anderweitig zu Prüfungszwecken vorgelegt und keine anderen als die angegebenen Hilfsmittel verwendet habe. Sämtliche wissentlich verwendete Textausschnitte, Zitate oder Inhalte anderer Verfasser wurden ausdrücklich als solche gekennzeichnet.

Ort, Datum

Unterschrift